2010

Conjugate Heat Transfer On A Gas Turbine Blade

Santiago Salazar
University of Central Florida

CONJUGATE HEAT TRANSFER ON A GAS TURBINE BLADE

by

SANTIAGO SALAZAR
B.S. University of Central Florida, 2005

A thesis submitted in partial fulfillment of the requirements
for the degree of Master of Science
in the Department of Mechanical, Materials and Aerospace Engineering
in the College of Engineering and Computer Science
at the University of Central Florida
Orlando, Florida

Fall Term
2010

ABSTRACT

Clearances between gas turbine casings and rotating blades is of quite importance on turbo machines since a significant loss of efficiency can occur if the clearances are not predicted accordingly. The radial thermal growths of the blade may be over or under predicted if poor assumptions are made on calculating the metal temperatures of the surfaces exposed to the fluid. The external surface of the blade is exposed to hot gas temperatures and it is internally cooled with air coming from the compressor. This cold air enters the radial channels at the root of the blade and then exists at the tip. To obtain close to realistic metal temperatures on the blade, the Conjugate Heat Transfer (CHT) approach would be utilized in this research. The radial thermal growth of the blade would be then compared to the initial guess.

This work focuses on the interaction between the external boundary conditions obtained from the commercial Computational Fluid Dynamics software package CFX, the internal boundary conditions along the channels from a 1D flow solver proprietary to Siemens Energy, and the 3D metal temperatures and deformation of the blade predicted using the commercial Solid Mechanics software package ANSYS.

An iterative technique to solve CHT problems is demonstrated and discussed. The results of this work help to highlight the importance of CHT in predicting metal temperatures and the implications it has in other aspect of the gas turbine design such as the tip clearances.

Dedicated to my Wife, Daughter, Dad, And Mom

ACKNOWLEDGMENTS

I would like to thank first of all my advisor, Dr. Divo, for his support during my academic years. His ability to explain complex engineering problems in simple and accurate terms has been quite encouraging and very helpful.

I consider myself lucky for having such great professors and in particular I would like to extend my gratitude to Dr. Alain Kassab for his continuous support and advice.

Working and going to school was always enjoyable and for that I would like to thank my mentor at work, Andreas Hadjinicolaou, and my direct manager, Bob Dorris, for his understanding, and constant support.

I wish to thank my family and extended family for their unconditional support, encouragement and for always creating such a lovely environment around me.

Finally, I would like to thank my dear wife and daughter, for their unconditional love, patience and support.

TABLE OF CONTENTS

LIST OF FIGURES

LIST OF ABBREVIATIONS

d:	Diameter of channels, m
h:	Heat Transfer coefficient, or convection conductance, $W/m^2.k$
L:	Length, mm
m:	Mass, kg
Nu:	Nusselt number, $h \cdot d / k$
Pr:	Prandlt Number, v / α
q'':	Heat flux, heat – transfer rate at surface per unit area, W/m^2
Q:	Mass transfer rate, kg/s
r:	Radius of channels, mm
Re:	Reynolds Number, $\rho V d / \mu$
S_t:	Stanton number, h / Gc
T_s:	Fluid temperature at the surface, K
T_m:	Metal temperature at the surface, K
T_{bulk}	*Fluid b*ulk temperature, K
u:	Mean velocity, m/s
u_∞:	Assigned velocity at any desired point, m/s
$\boldsymbol{V}$:	Axial velocity vector, $\vec{V}$, m/s
V:	Velocity magnitude, m/s
α:	Thermal diffusivity, $k / \rho \cdot c_{p,}\ m^2/s$
ρ:	Fluid density, kg/m^3
μ:	Dynamic viscosity, $N\,s / m^2$

v:	Kinematic viscosity, μ / ρ, m

CHAPTER ONE: MOTIVATION AND HYPOTHESIS

Standard practices to solve heat transfer problems on gas turbine components may not be adequately predicting metal temperatures. One factor for this to take place is the enormous amount of time that takes to set up a sufficient mesh that can be capable of producing reliable solutions when simultaneously solving the Navier-Stokes equations for the flow and the conduction for the solid. Another factor worth to be mentioned is the tedious labor involved in putting results files in formats that can be read by the solvers implicated in the calculations. In addition to the above interpolation techniques have to be used simultaneously in order to share information accurately between the conduction solver mesh and the flow solver mesh. So, when dealing with 3-D CHT problems, typically it is standard practice for each flow domain to be treated and solve independently and solutions never couple or fed back to the others solvers proficiently to form an efficient loop that can be capable of generating results close to actual experience. When failing to deal properly with a full 3D CHT problem such as the ones presented in most of the internally cooled gas turbine components metal temperatures are predicted incorrectly by several degrees, a debit is paid on calculating the life of the part, blade tip clearances may be over or under predicted, and the overall gas turbine efficiency might be compromised.

CHAPTER TWO: LITERATURE REVIEW AND BACKGROUND

Gas turbines are rotary engines mainly used for aircraft propulsion and in land-based power generation. As main components, a simple cycle gas turbine has the compressor, combustor and turbine. The compressor that is located up stream of the turbine compresses the air increasing its pressure and temperature. Fuel is then mixed with air in the combustion section and ignited. This combustion produces a tremendous increase in energy where velocity, temperature and pressures of the working fluid are radically increased. This high energy fluid is directed through the stationary vanes over turbine blades and produces a rotational movement or spinning of the shaft that simultaneously assist to power the compressor. The shaft power output of the turbine depends on how much energy is extracted when expanding the hot gases passing through its vanes and blades and how successful this expansion is in reducing its exhaust temperature. The shaft power is then used among many other effects to power a generator for the production of the increasingly needed electric power. This increasing need over the past couple of decades has motivated the call for creative ways to increase efficiency and power out put.

Typically, efficiency and power out put are increased with turbine inlet temperatures. These temperatures are normally above material melting point of the parts and it is because of these high temperatures that sophisticated cooling schemes are extremely important. Along, with these sophisticated cooling schemes, thermal barrier coatings

have as well been developed in the recent decades and are commonly used with internal cooled parts to increase part life.

As mentioned above, modern gas turbine blade components are equipped with internal cooling features in order to withstand the high gas temperature at which they have to operate. The internal cooling is design to extract the heat from the internal walls and cool it significantly to maximize the life of the component. These cooling features in the turbine components affect part life and efficiency. So having ways to predict accurate metal temperatures is crucial. Too much cooling and the engine will pay a price on efficiency. Not enough cooling and the part life decreases and gets compromised. Furthermore, this extreme working environment produces intense stresses due to the high rotating speeds and thermal gradients. In addition, in order to achieve or increase efficiency the tip clearance between the gas turbine casing and the tip of the blade have to be maintained as minimum as possible and therefore play a very important roll on gas turbines power out put.

In order to predict a more realistic radial thermal growth and/or tip clearance of the blade, conjugate heat transfer effects on internally cooled turbine components have to be taking into account. The interaction at the intersection between different domains in particular one of a moving fluid and solid is said to be set for a conjugate heat transfer problem as is the case for most modern gas turbine components. The temperatures solution at this intersection is coupled in a way that the energy and conduction equations of the fluid and solid respectively have to be solved in an iterative way. Once the metal temperatures at

these different domain intersections are found iteratively the radial growth of the blade could be predicted more realistically and life of the part can be predicted with confidence. CHT problems have been studied intensively in the past couple of decades and now with the use of sophisticated software packages and powerful computers more difficult and complex problems are solve faster and more accurately. This work focuses on the interaction between the external boundary conditions obtained from the commercial Computational Fluid Dynamics software package CFX, the internal boundary conditions along the channels from a 1D flow solver proprietary to Siemens Energy, and the 3D metal temperatures and deformation of the blade predicted using the commercial Solid Mechanics software package ANSYS.

The blade used in this work belongs to the SGT6-3000E class engine (figure 1). It features a 19-stage axial flow compressor, 14 can-type combustor in a circular array and a four-stage turbine. It has a gross power output of 121MW and a gross efficiency of 34.7%.

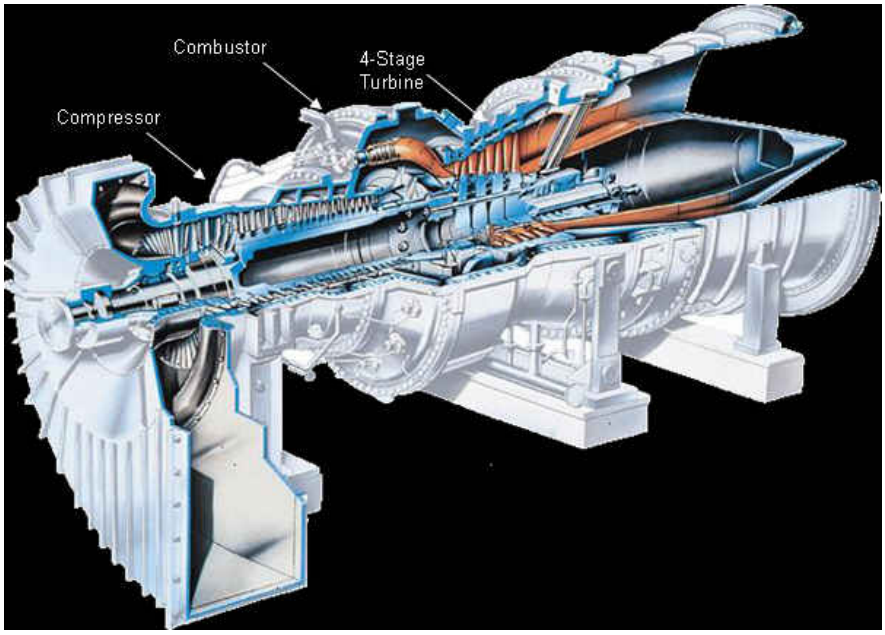

Figure 1: SGT6-3000E Gas Turbine 60 Hertz Application

The Pro-E model of the second stage blade used for this work is shown in figure 2. Figure 3 shows the tip of the blade which has a shroud design with the purpose of minimizing the hot air going over and circumventing the blade tip.

Figure 2: Blade 2

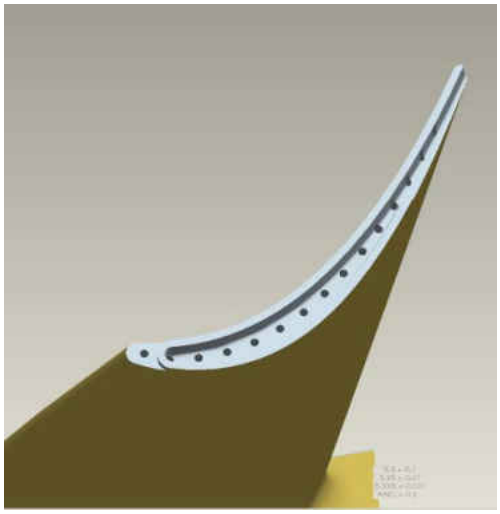

Figure 3: Blade 2 Tip

The fluid used to cool the part is air coming from the earliest stages of the compressor. The blade has fifteen radial channels dedicated for internal cooling (see figure 4). They have their inlet at the root of the blade and exit at tip of the blade.

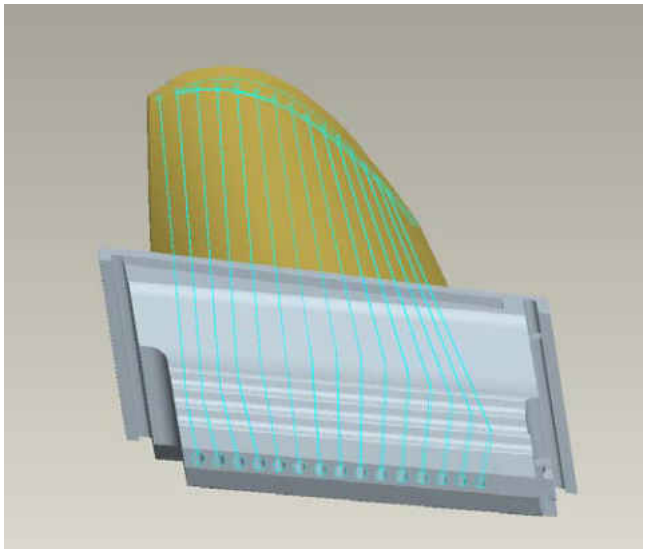

Figure 4: Radial channels for cooling

CHAPTER THREE: RESEARCH METHODS

3.1 Iterative Looping:

The approached taken to obtained the external boundary conditions for the 3D CHT problem is shown in figure 5. The external flow field inlet and outlet conditions are specified and an adiabatic wall assumption is made at the blade airfoil wall. The compressible Navier-Stokes (NS) equation is then solved for the external fluid region and a temperature profile is obtained for the airfoil. Assumptions for metal temperatures are made, the compressible NS are then solved again and then heat transfer coefficients and bulk temperature obtained.

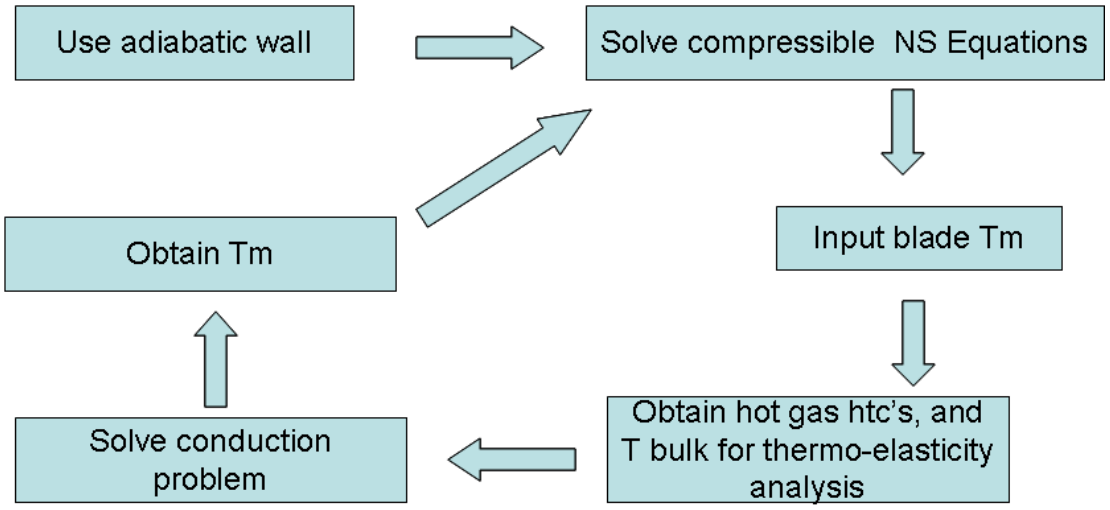

Figure 5: External loop

The approached taken to obtained the internal boundary conditions for the problem are shown in figure 6. Internally, supplied inlet, exit pressures and temperatures are specified and internal channel walls temperatures guessed. With this inputs the 1D compressible NS are solved and in effect gives the fluid bulk temperature and the heat transfer coefficient in the channel.

These bulk temperature and heat transfer coefficients that were obtained for the internal and external fluid are fed as inputs to the conduction model in ANSYS. Once these boundary conditions are imposed to the model the metal temperatures distributions for the stage two rotating blade is obtained. The metal temperatures obtained from the conduction model are then used as inputs for the 3D and 1D fluid models and the process is repeated until the new metal temperatures found converge. In addition, at the end of each loop, the resultant metal temperatures distribution along with load pressures and centrifugal forces are used for the thermo-elasticity assessment and the blade growth monitored.

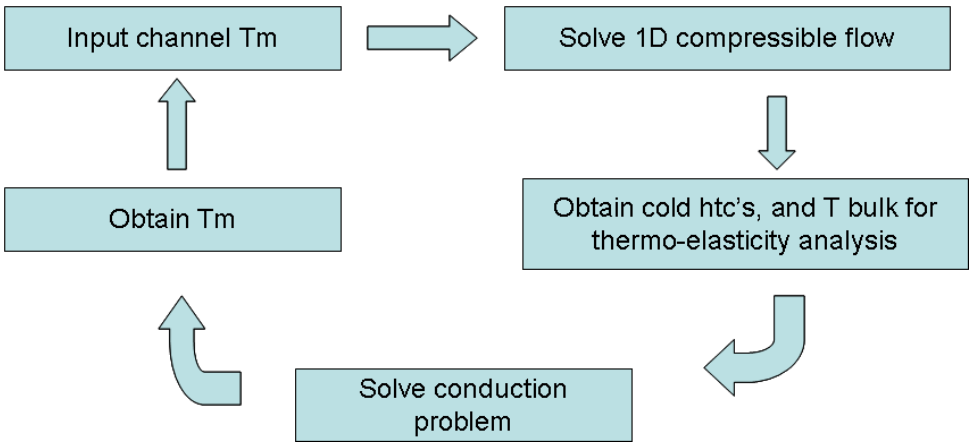

Figure 6: Internal loop

3.2 Cooling Boundary Conditions: K1D

Cooling holes dimensions and geometry used to build the internal cooling channels are shown in figure 7.

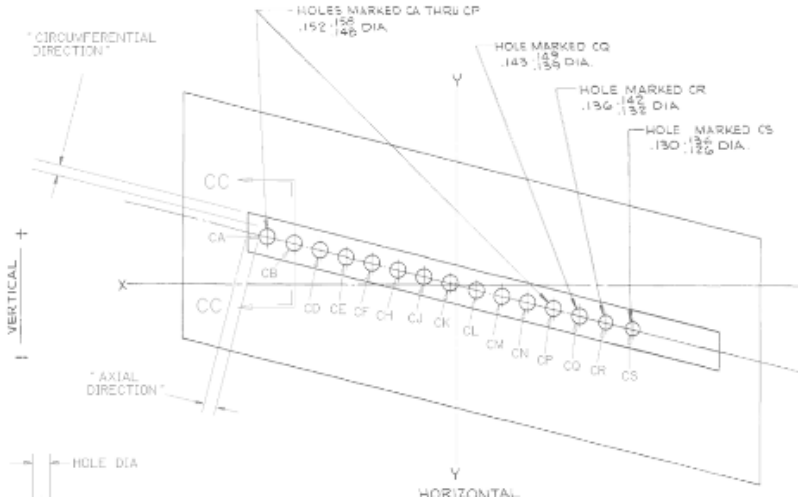

(a)

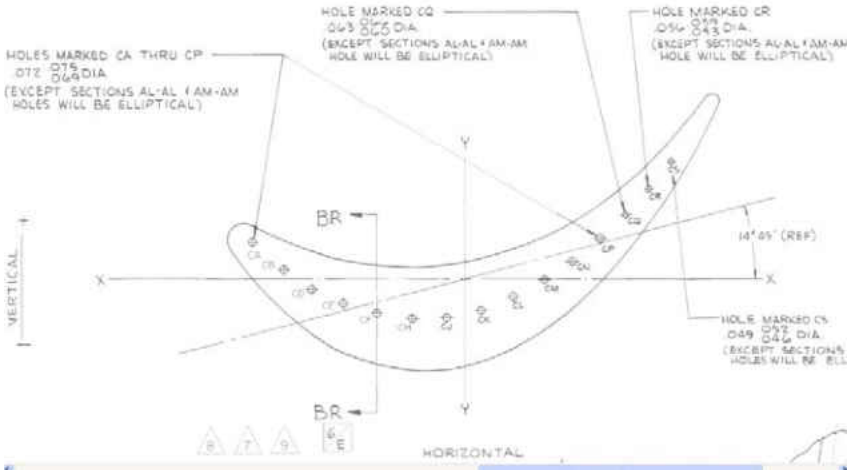

(b)

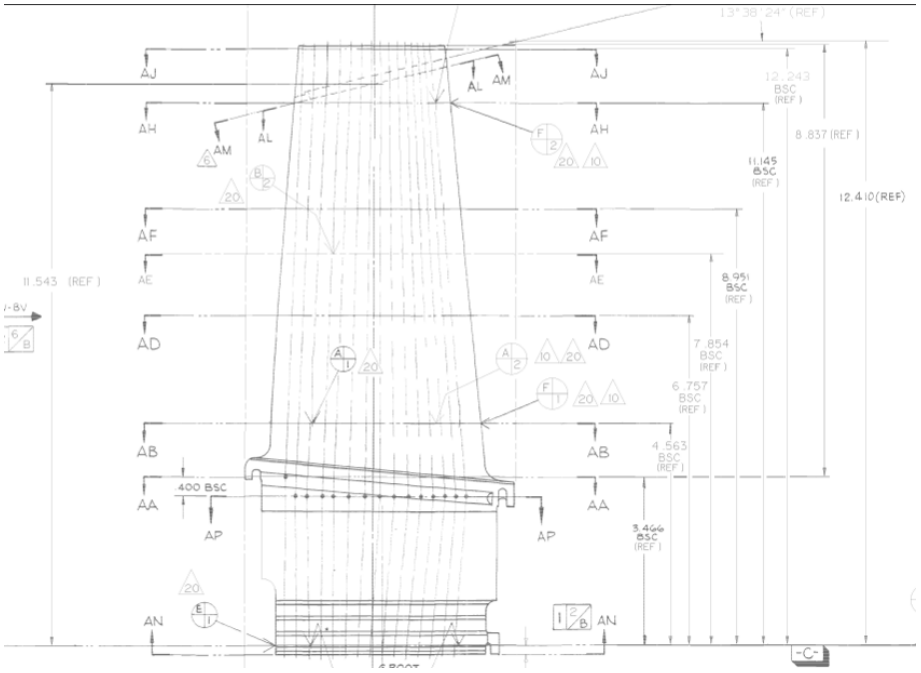

(c)

Figure 7: Blade geometry information in inches (a) cooling holes at blade inlet (b) cooling holes at airfoil section (c) radial dimensions

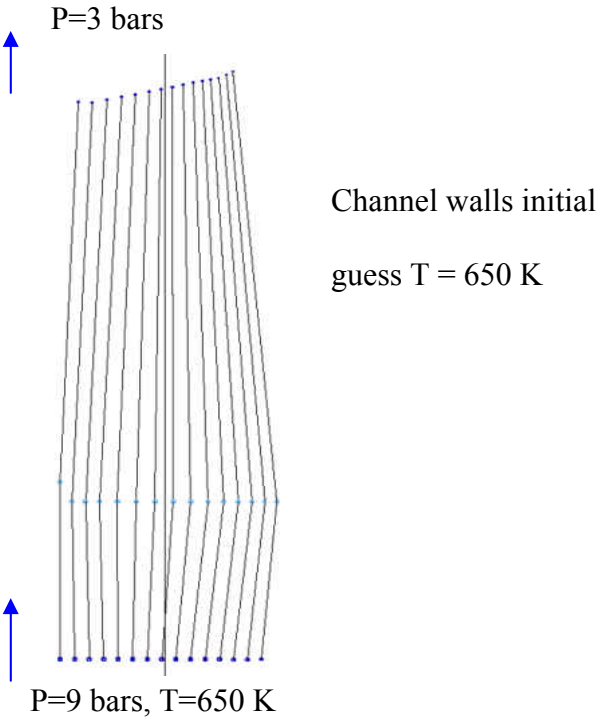

Figure 8: Internal Flow model and boundary conditions

The geometrical information is used to build the internal flow network in the 1D flow solver where the channels are treated as smooth ducts with turbulent flow and entrance effects on overall heat transfer. Supplied inlet and exit pressures are specified along with inlet and wall temperatures of the channels. The inlet and exit pressures used for the internal cooling were 9 and 3 bars respectively. The inlet temperature and the initial temperature for the wall channel used was 650 K. Air properties in the channel are calculated taking into account area variations, wall friction, rotation and heat transfer. The internal flow network is shown in figure 8. The flow traveling radially upward through the channel sees its density change from inlet to outlet due to the heat pick up from the walls. For a heated channel the outlet density is smaller than inlet density $\rho_{out} < \rho_{in}$ and for the sections of constant channel areas the inlet velocities is less that the outlet velocity $V_{in} < V_{out}$. Continuity is maintained through the channel such that $\dot{m} = \rho VA$ at every point in the channel

$$G = \frac{\dot{m}}{A} \tag{1}$$

On the contrary momentum $\dot{m}(V_{out} - V_{in})$ needs to be balanced due to the velocity differences at the channel's inlet and outlet by the pressure difference

$$\Delta P_{acc} = G^2\left(\frac{1}{\rho_{out}} - \frac{1}{\rho_{in}}\right) \tag{2}$$

Empirical correlations are used to account for the pressure loss due to wall friction and adding this effect the pressure drop across a straight portion of the channel the pressure drop for the constant channel section takes the form

$$\Delta P_s = f\frac{4L}{D_h}\frac{1}{2}\rho V^2 + \Delta P_{acc} \tag{3}$$

Where f is the friction factor, D_h is hydraulic diameter and ρ is the average of the inlet and outlet densities.

Contractions effects are taking into account as well and for air contracting from a large area A_a to a smaller area A_b this can be put in the form

$$P_a - P_b = \left(1-\sigma_{a-b}^2\right)\frac{1}{2}\rho_b V_b^2 + K_c\frac{1}{2}\rho_b V_b^2 \tag{4}$$

Where σ_{a-b} is the passage contraction ratio

$$\sigma_{a-b} = \frac{A_b}{A_a} \tag{5}$$

And K_c is the contraction loss coefficient.

In the same manner expansion effects from a small area A_c to a large area A_d in the channel can be put in the following equation

$$P_d - P_c = \left(1-\sigma_{c-d}^2\right)\frac{1}{2}\rho_c V_c^2 + K_e\frac{1}{2}\rho_c V_c^2 \tag{6}$$

Where K_e is the enlargement loss coefficient and σ_{c-d} is given by

$$\sigma_{c-d} = \frac{A_c}{A_d} \tag{7}$$

The effects of heat addition in the channel are measured by empirical correlations of the Stanton number S_t. The Stanton number is a dimensionless number that relates the ratio of the heat transfer coefficient to the thermal capacity of the fluid C_p

$$St = \frac{h}{C_p \rho V} \tag{8}$$

This relation can also be used in conjunction with the Nusselt number Nu, the Reynolds number Re and the Prandtl number Pr

$$St = \frac{Nu}{\mathrm{Re}\,\mathrm{Pr}} \tag{9}$$

3.3 Computational Fluid Dynamics Solver: CFX

Figure 9 and 10 shows the inlet and outlet boundary conditions profiles for the flow domain as a function of radial position. The maximum total pressure and temperature at the inlet are 716,000 Pa and 1250 K respectively. At the outlet the maximum static pressure and temperature are 380,000 Pa and 1,250 K respectively.

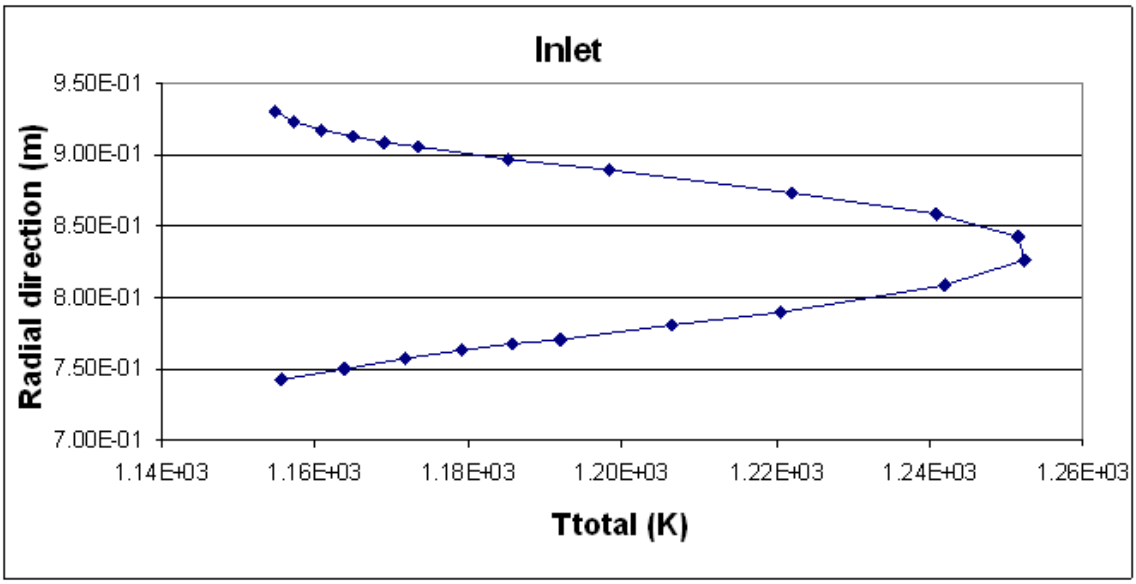

(a)

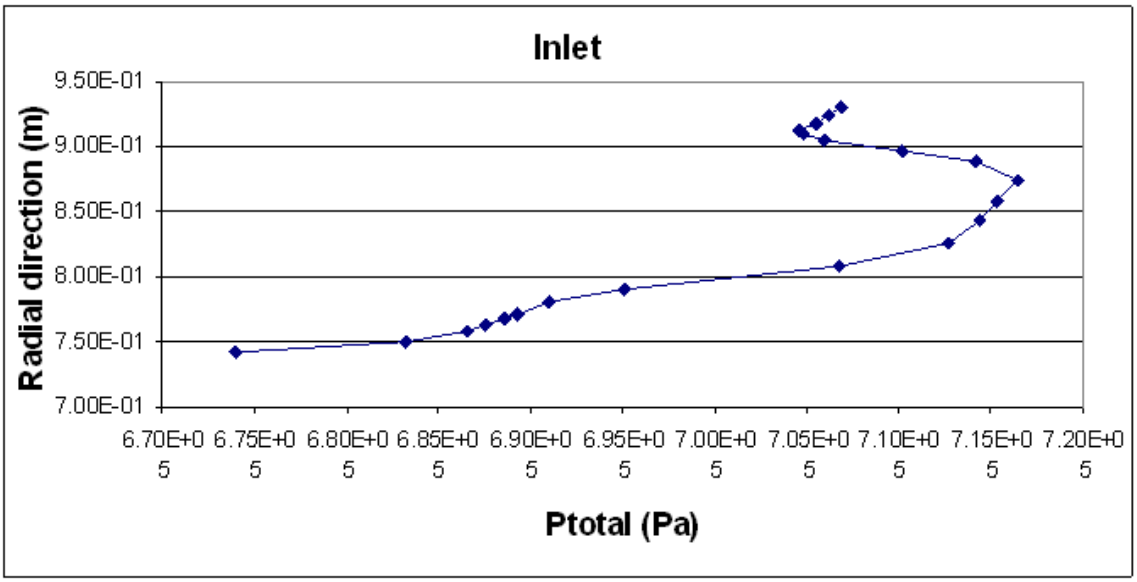

(b)

Figure 9: Inlet conditions (a) Total Temperature (K) (b) Total Pressure (Pa)

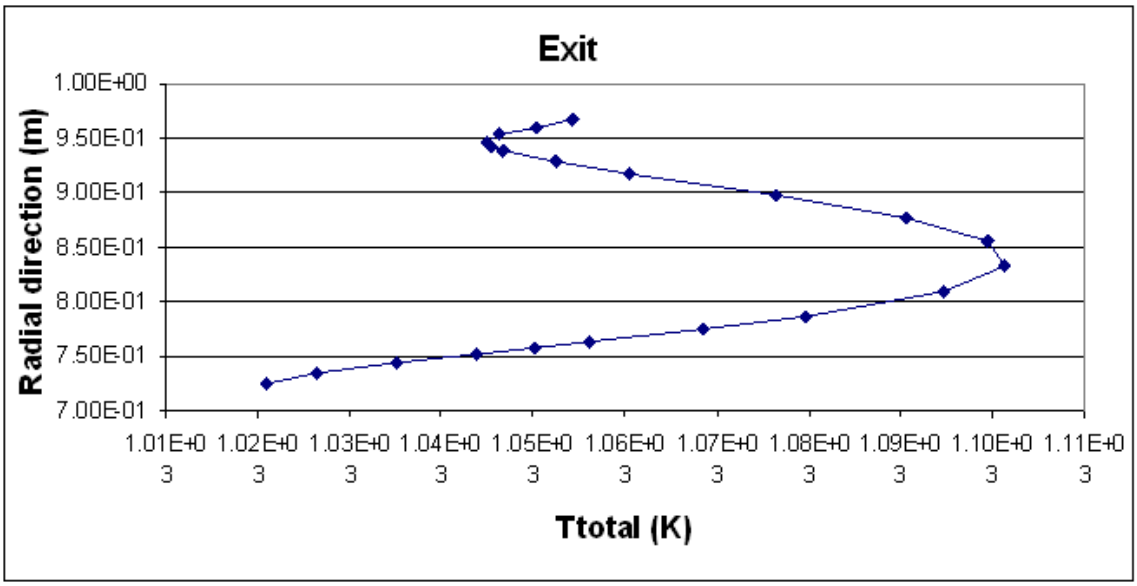

(a)

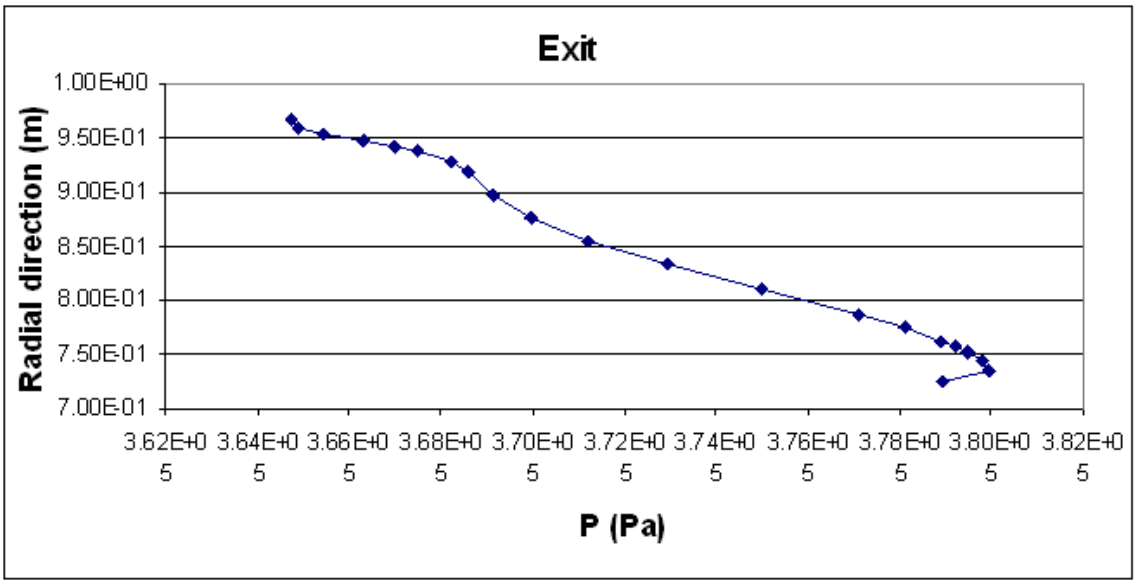

(b)

Figure 10: Outlet conditions (a) Total Temperature (K) (b) Static Pressure (Pa)

The domain and domain boundary conditions of the main flow are shown in figure 11. The basic dimensions of the flow domain are 69 mm in width, 187 mm in length and, 190 mm of height at the inlet and 243 mm of height at the exit. The structured mesh uses 454,145 number of nodes, 435,456 number of elements, 435,456 total number of hexahedrons, and 77472total number of faces.

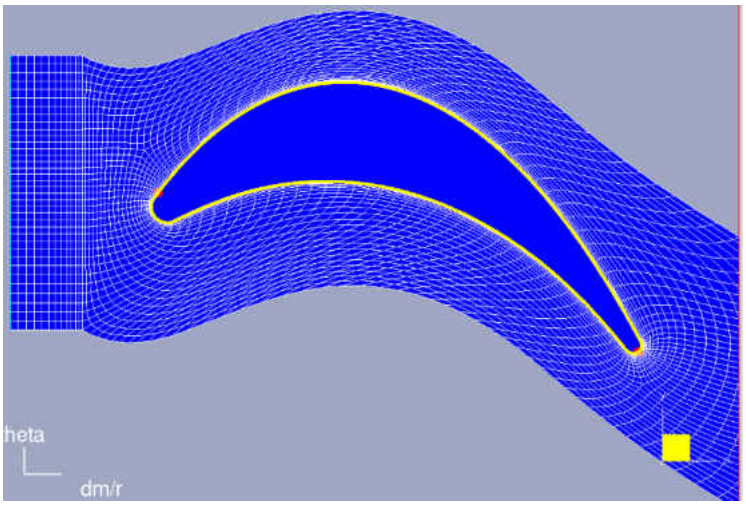

(a)

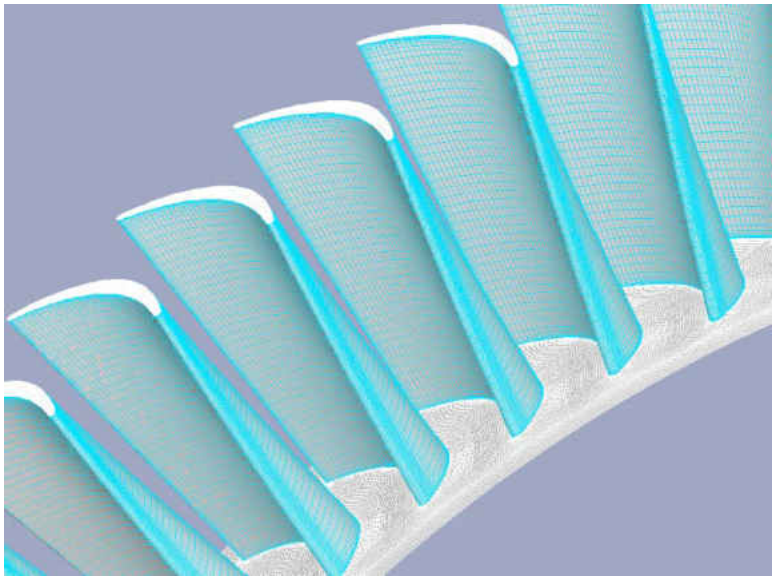

(b)

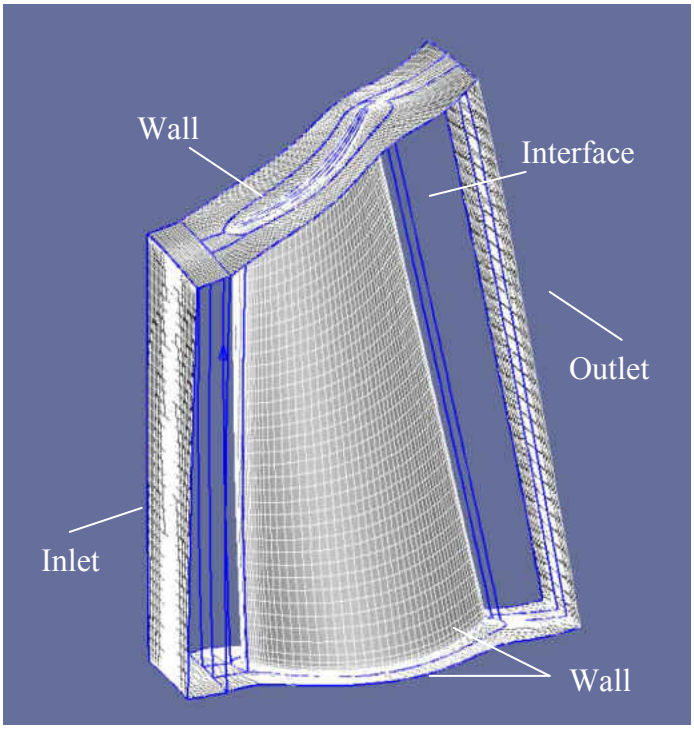

(c)

Figure 11: Computational grid (a) end walls (b) domain periodicity (c) domain boundaries

The motion and heat transfer of the fluid in the flow-field are described by the compressible NS equations and can be expressed in the form of continuity, momentum and energy equations.

The continuity equation can be expressed as

$$\frac{\partial \rho}{\partial t} + \nabla \cdot \left(\rho \vec{V}\right) = 0 \tag{10}$$

The momentum equation describing the force balances of the fluid can be expressed as

$$\frac{\partial \left(\rho \vec{V}\right)}{\partial t} + \nabla \cdot \left(\rho \vec{V} \vec{V}\right) = -\nabla p + \nabla \cdot \underline{\underline{\tau}} \tag{11}$$

Where $\underline{\underline{\tau}}$, is the stress tensor.

Based on the first law of thermodynamics the energy equation can be put in the following form

$$\frac{\partial(\rho h_{tot})}{\partial t} - \frac{\partial p}{\partial t} + \nabla \cdot (\rho u h_{tot}) = \nabla \cdot (k \nabla T) + \nabla \cdot (u \tau) \tag{12}$$

Where h_{tot} is the total enthalpy

$$h_{tot} = h + \frac{1}{2}\left|\vec{V} \cdot \vec{V}\right| \tag{13}$$

And k is the thermal conductivity

The solution of the Navier-Stokes equations for non ideal flows is obtained by applying the finite volume methodology. This method evaluates the continuity, momentum and energy equations as algebraic approximations and then solves them by applying numerical methods.

Turbulence in the flow field is dealt by the use of the Eddy Viscosity Turbulence Models. Under this category the Two Equation Turbulent Model is used since they offer a good compromise between numerical effort and computational accuracy. The Two Equation Turbulence Model used for this simulation was the Shear Stress Transport (SST). The $k-w$ based SST model is known to accurately predict the amount of flow separation under adverse pressure gradients.

3.4 Thermo-Elastic Solver: ANSYS

The blade material used for thermo-elastic analysis was a nickel-base alloy IN738LC. figure 16 shows the mesh used in Ansys. Solid element 87 was used for the thermal solution, along with surface effect elements 152. The structural analysis uses the same mesh as the thermal analysis and it was solved using solid element 92 and surface 154. Solid87 is a 3-D 10-node tetrahedral thermal solid particularly used to model irregular meshes. Element Solid 87 possesses one degree of freedom, temperature, at each node. Figure 12 shows the geometry of element Solid 87, nodes location and coordinate system.

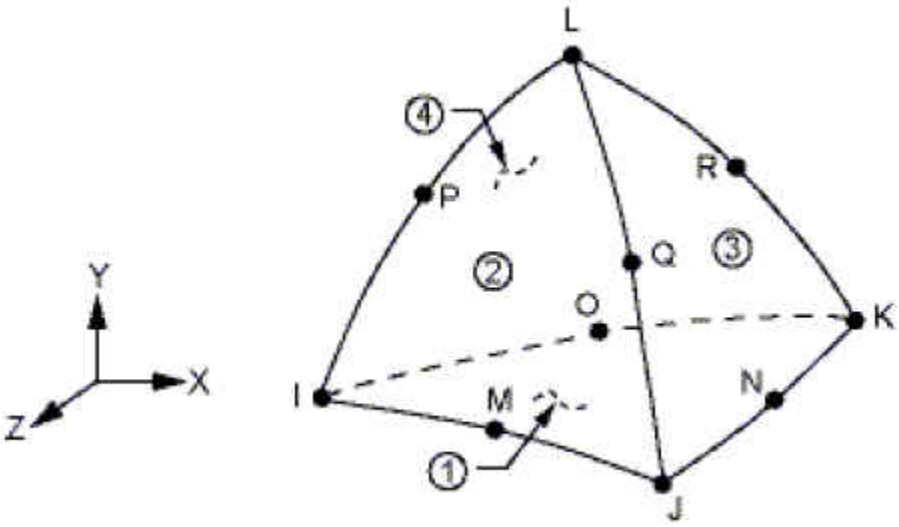

Figure 12: Solid 87 geometry

When the same model containing Solide87 is also to be analyzed structurally is typically replaced by a 10-node tetrahedral structural solid element, Solid 92. This element has three degrees of freedom at each node: translations in the nodal x, y, and z directions. Figure 13 shows the element geometry.

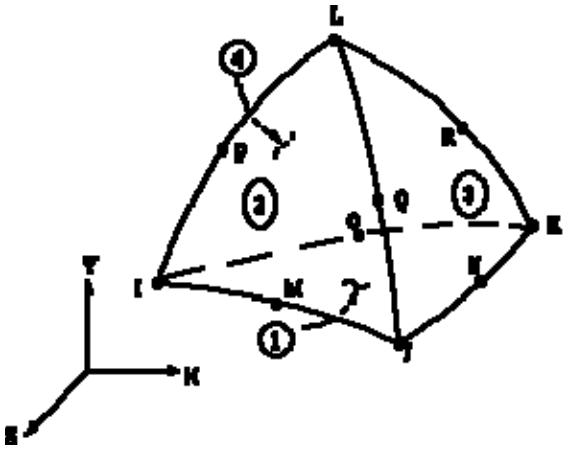

Figure 13: Solid92 geometry

SURF152 is a surface effect element overlaid onto the area face of any 3-D thermal element and the geometry, nodes and coordinate system are shown in figure 14.

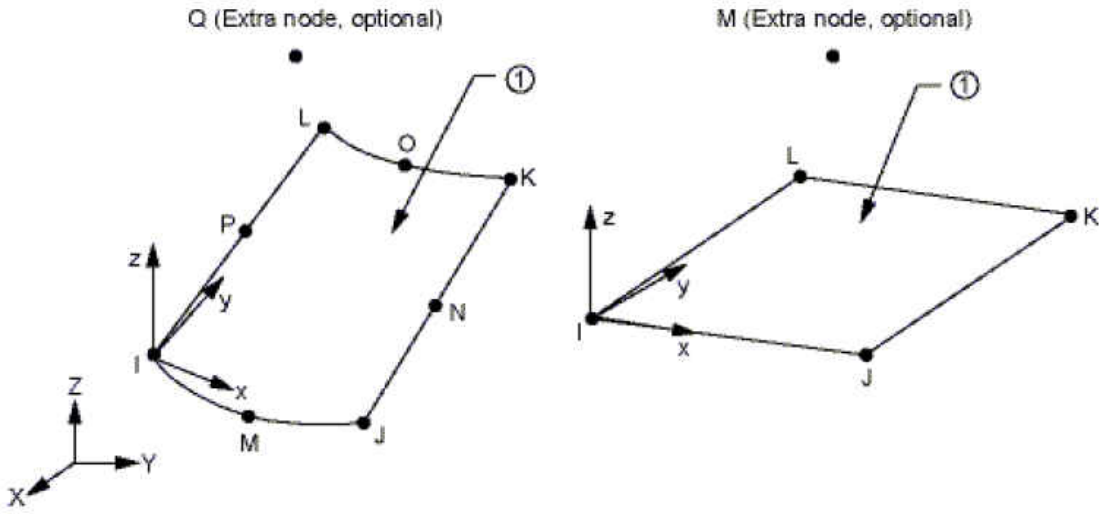

Figure 14: SURF152 geometry

SURF154 is a surface effect element overlaid onto the area face of any 3-D structural element and the geometry, nodes and coordinate system are shown in figure 15.

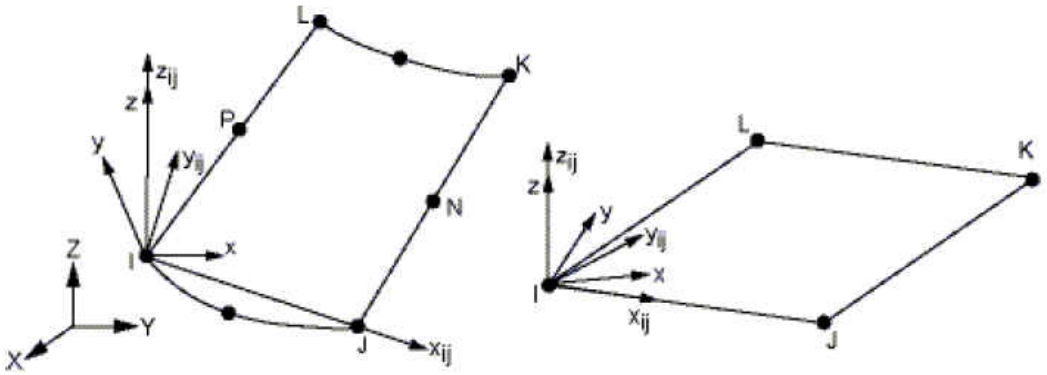

Figure 15: SURF154 geometry

The blade geometry was poorly constructed on some critical areas as the blade root serrations, and the blade tip. More over in order to effectively mesh the cooling hole channels and to refine the areas mention above more elements had to be added to refine the mesh. The total number of elements used was 673,425 and the total number of nodes 866,637.

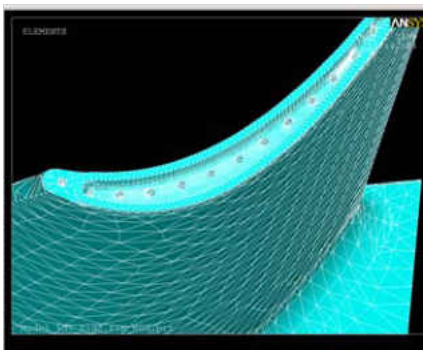

(a)

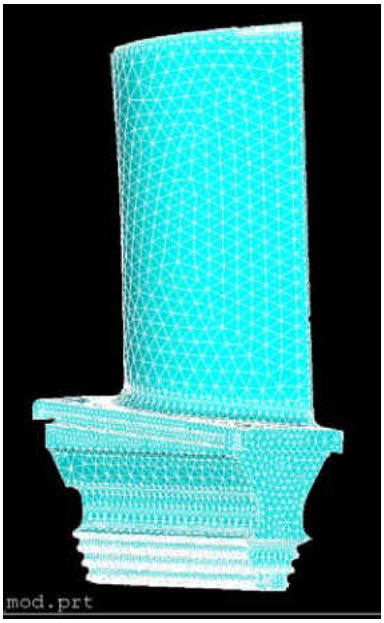

(b)

Figure 16: FEA mesh (a) tip close up (b) blade 2

The internal and external heat transfer coefficients and bulk temperatures imposed on the blade to assess the metal temperatures were taken from the 1D and CFX solutions respectively. A metal temperature of 400 ^{o}C was used for the blade root along with an *h* of 0.5 mW/mm^2K

The governing equation for the conduction problem is

$$\nabla \cdot [k(T_s)\nabla T_s] = 0$$

Where T_s represents the blade surface temperatures and *k* is a function of the metal temperature.

After solving for the metal temperatures a structural analysis is perform using the thermal solutions as body loads. The blade was constraint at the root serrations circumferentially

and radially and it was constraint axially at the aft bottom hook as shown in figure 13. More over, the effect of the blade rotation was modeled by indicating an angular velocity on the z axis.

The technique to solve the thermo-elasticity problem is known as Finite element Analysis (FEA). This method discretizes the domain into sub-domains called elements. Assumes a function that describes the behavior of the element, assembles the elements properties to obtain the system equations, imposes boundary conditions and solve the system equations.

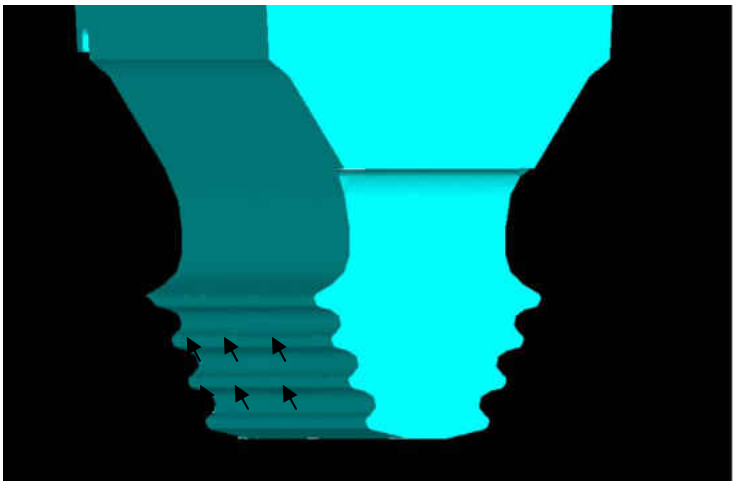

(a)

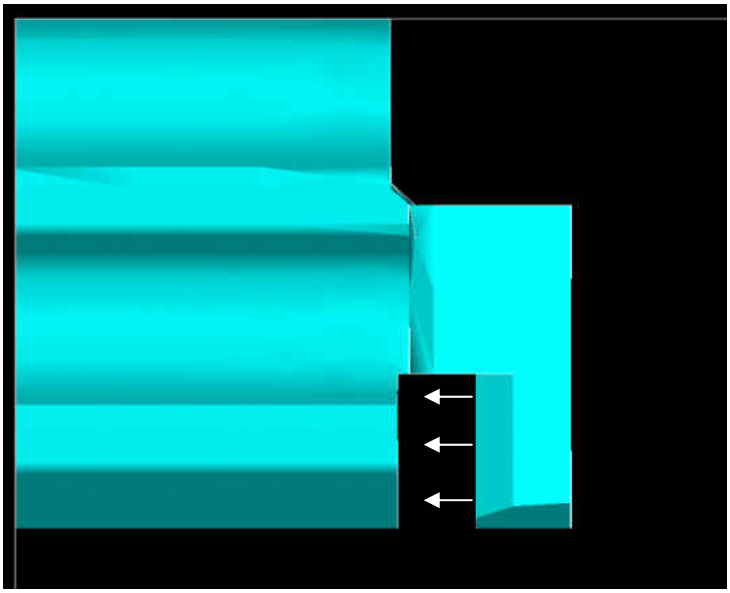

(b)

Figure 17: Blade constraints (a) radial and circumferential (b) axial

CHAPTER FOUR: RESULTS AND DISCUSSIONS

4.1 Conjugate Convergence

It takes over 128 iterations to solve the equations in the flow domain and it takes approximately 5,729 seconds of CPU time to achieve convergence criteria. A snap shot in time of the turbulence model convergence is shown in figure 14.

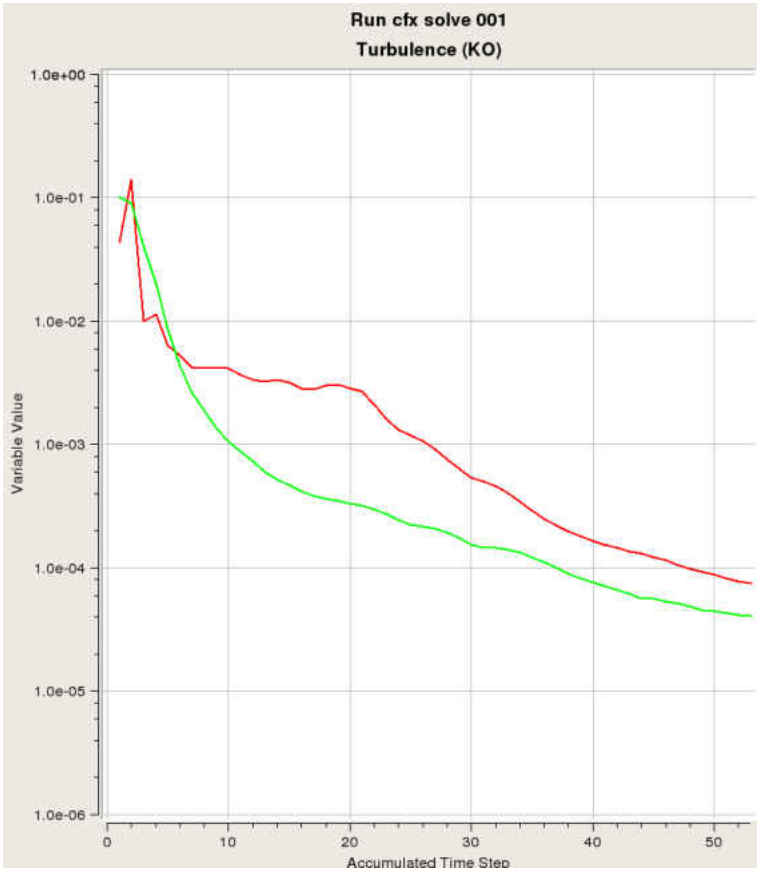

Figure 18: Turbulence model convergence

The conduction model takes 4,980 seconds of CPU time to converge while the convergence time from the 1D solver is negligible compared to the flow and conduction models.

The L2 norms of the five thermal loops are shown in figure 19. The metal temperatures become stable after fifth iteration.

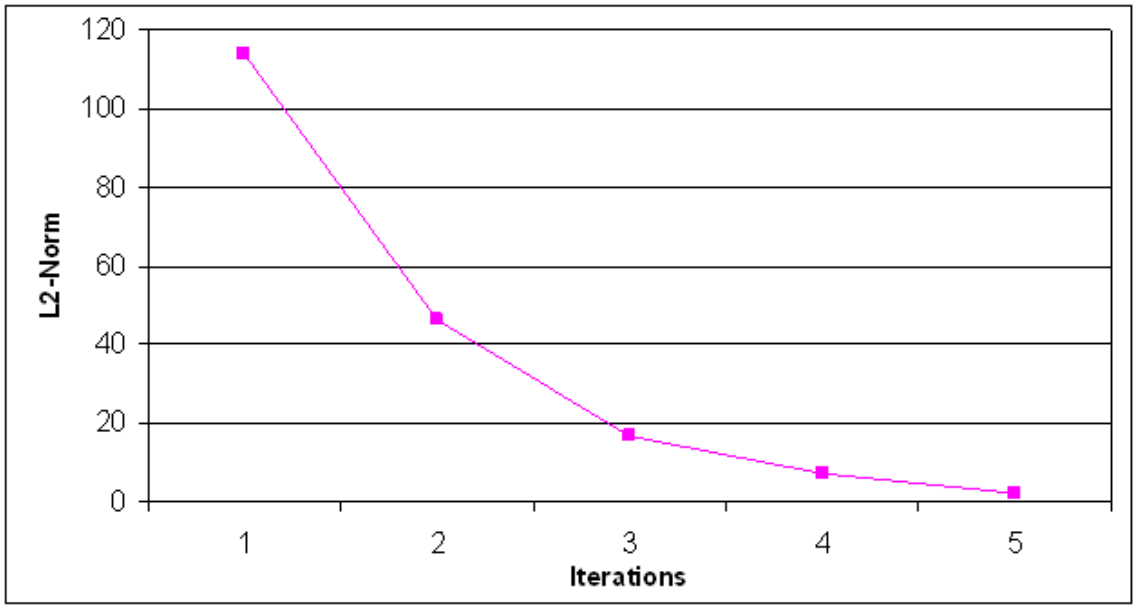

Figure 19: L2 norm

The average tip clearance of the blade is 4.11 mm. Figure 20 shows the radial growth of the blade after every thermal loop. The radial displacements are steady after the third iteration and compared to the first iteration the growth is under predicted by 0.211 mm.

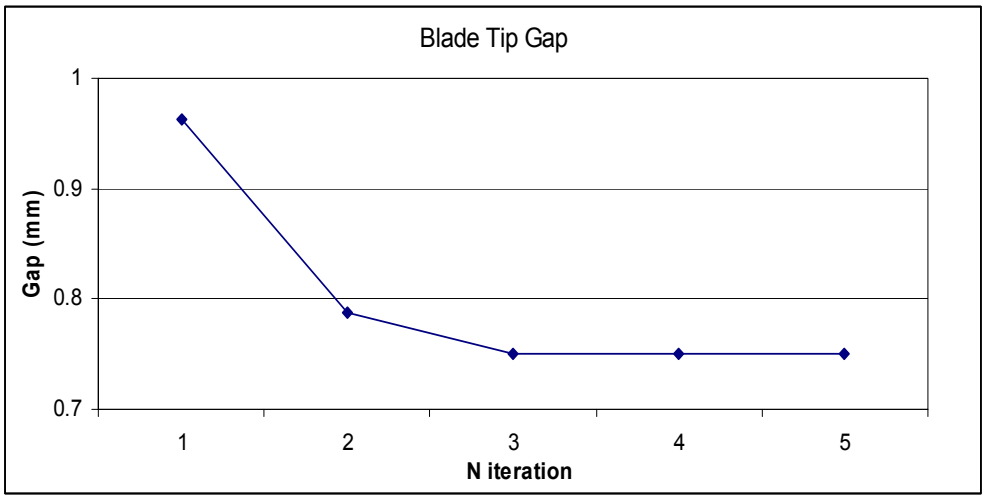

Figure 20: Gap clearance at blade tip

4.2 1D Cooling Network Solution

The airfoil channels bulk temperature and heat transfer coefficient results for the first and last iteration are shown in figure 21. The average heat pick up is approximately 200 K and the average heat transfer coefficient is approximately 2,700 W/m^2K

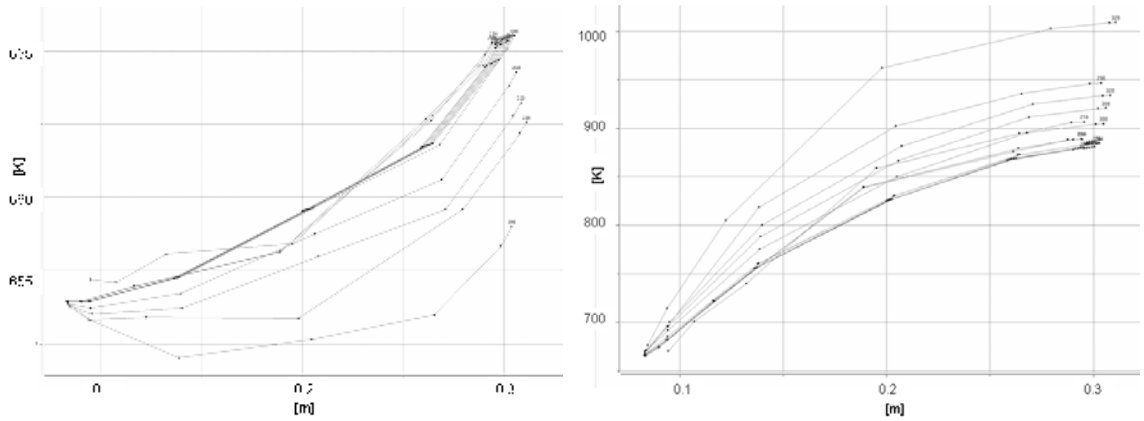

(a)

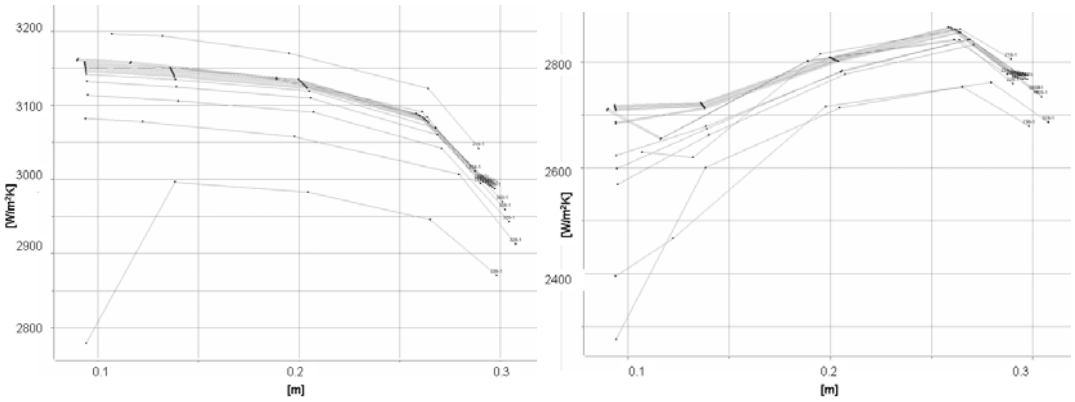

(b)

Figure 21: Internal results for first and last iterations (a) bulk temperature (b) heat transfer coefficients

4.3 Volumetric CFD Solution

Figure 22 shows the fluid pressure, temperature and mach number results from CFX solution. High pressure regions are seen at the stagnation point and in the airfoil pressure side; the airfoil suction side shows the lower pressures as expected. Unlike the pressure distribution the mach numbers on the fluid domain are low on the pressure side and high on the suction side of the blade. The results also show that the fluid total temperature for the first loop is higher near the airfoil walls than the last loop. Figure 23 shows the pressure contours on the blade airfoil that will be used as boundary conditions for the thermo-elasticity problem. The maximum pressure seen is approximately 5.6 MPa and is located on the airfoil pressure side. Figures 24 through 25 show the gas heat transfer coefficients and the bulk temperature at the airfoil, and tip of the blade.

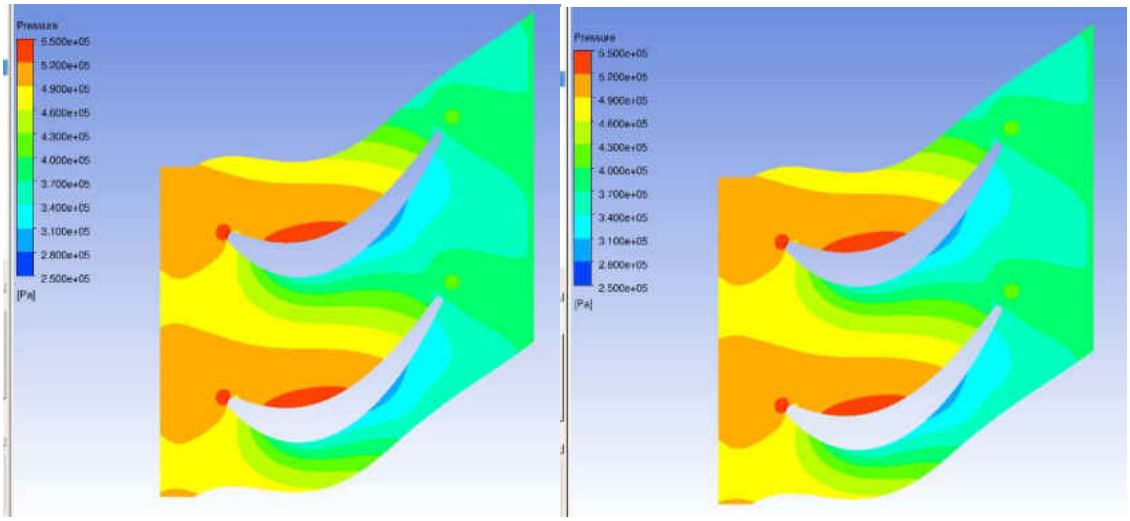

(a)

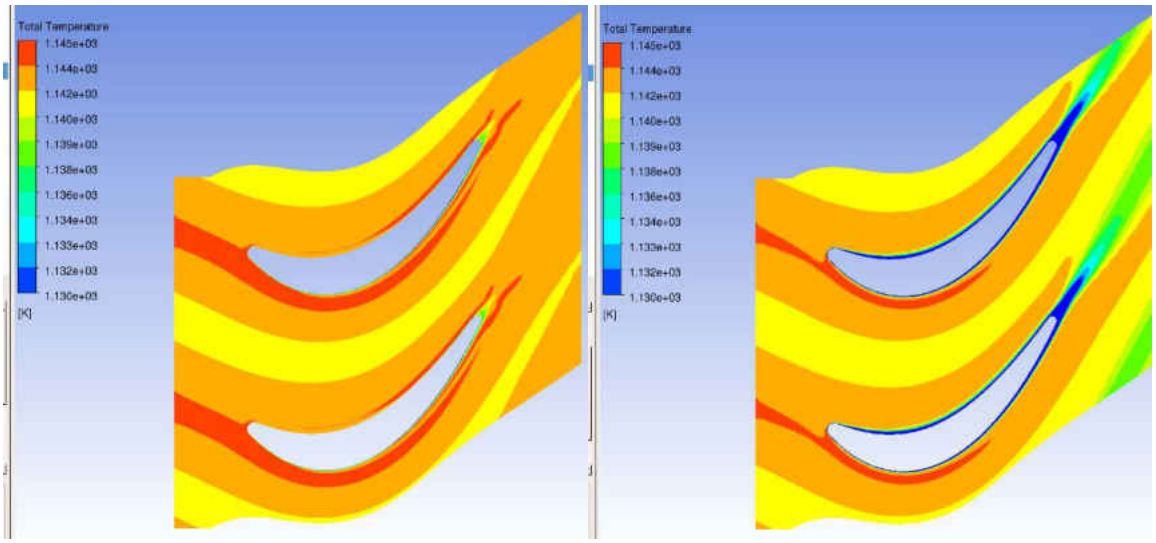

(b)

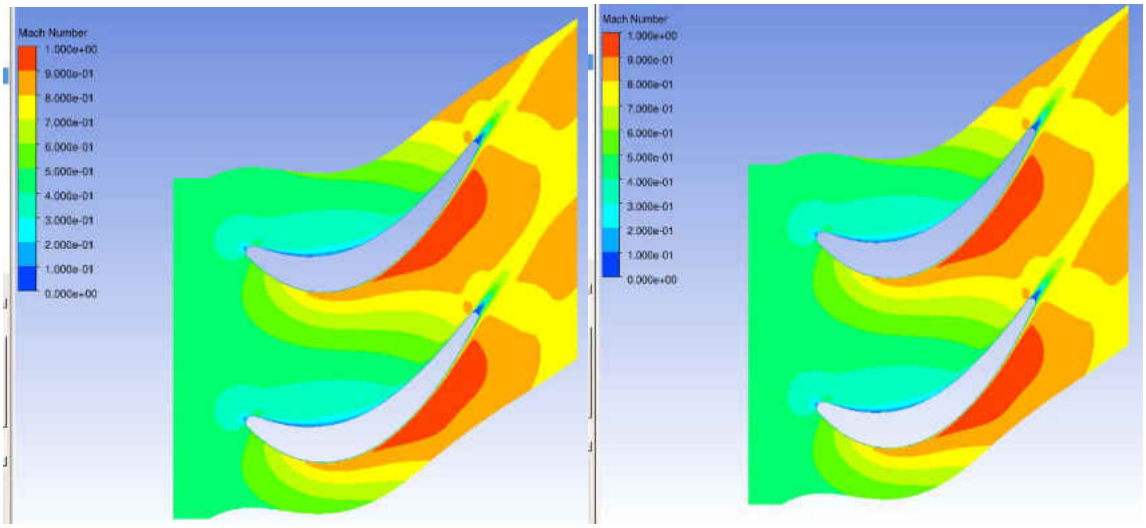

(c)

Figure 22: First and last iteration, (a) pressure (b) temperature (c) mach number

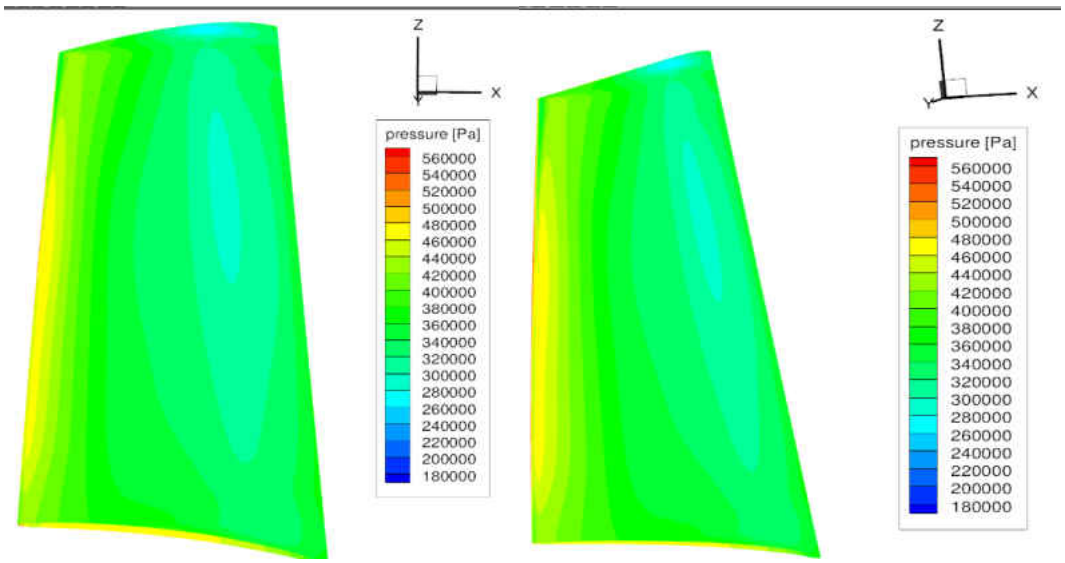

(a)

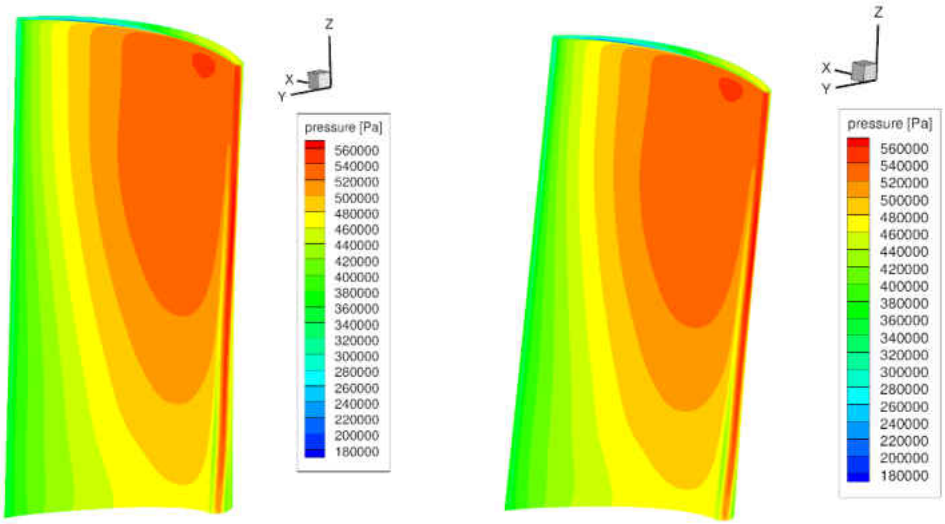

(b)

Figure 23: First and last iterations, pressure contours, (a) suction side (b) pressure side

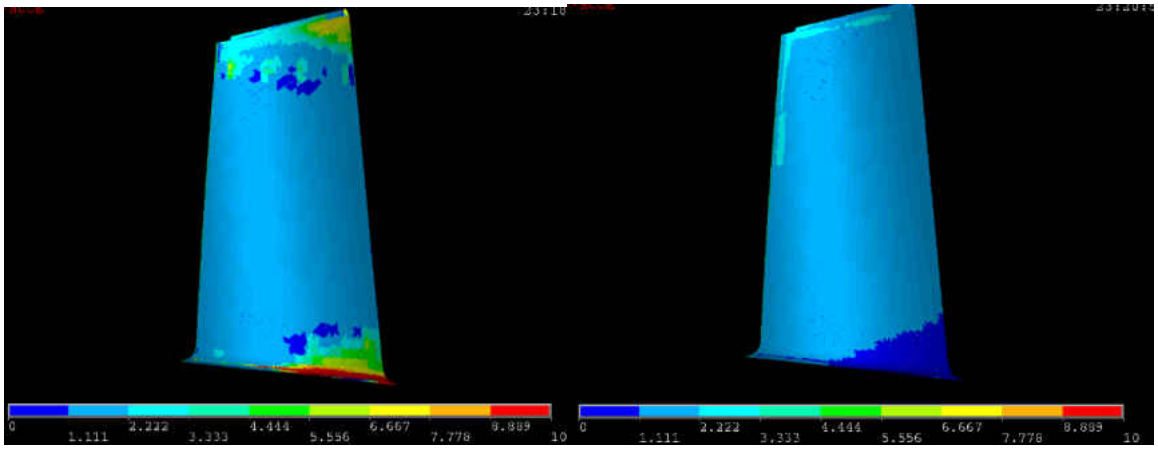

(a)

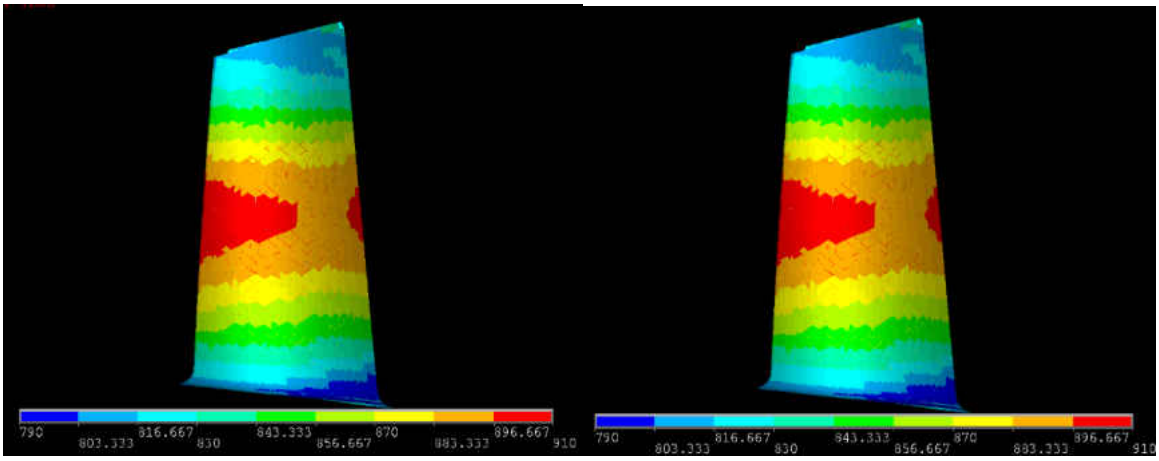

(b)

Figure 24: First and last Iteration, (a) airfoil heat transfer coefficient (mW/mm^2K) (b) airfoil bulk temperature (^oC)

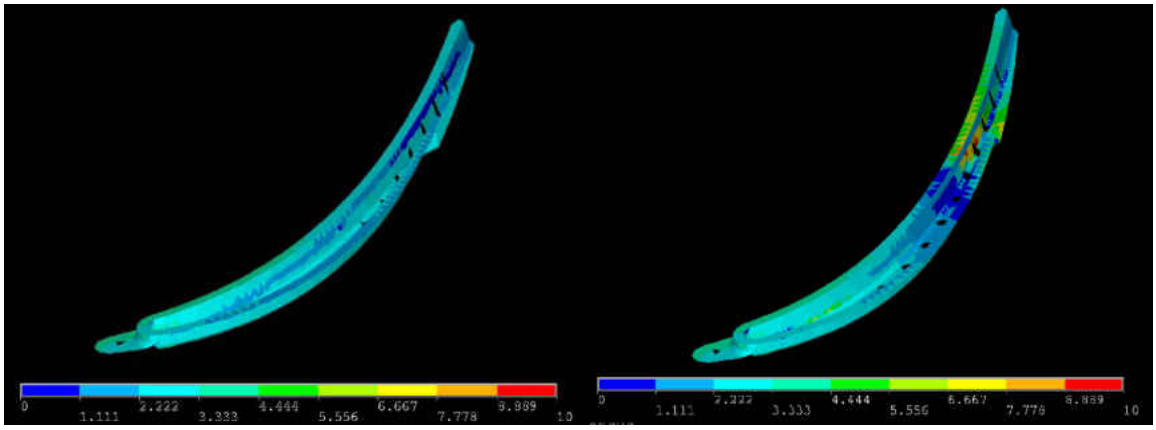

(a)

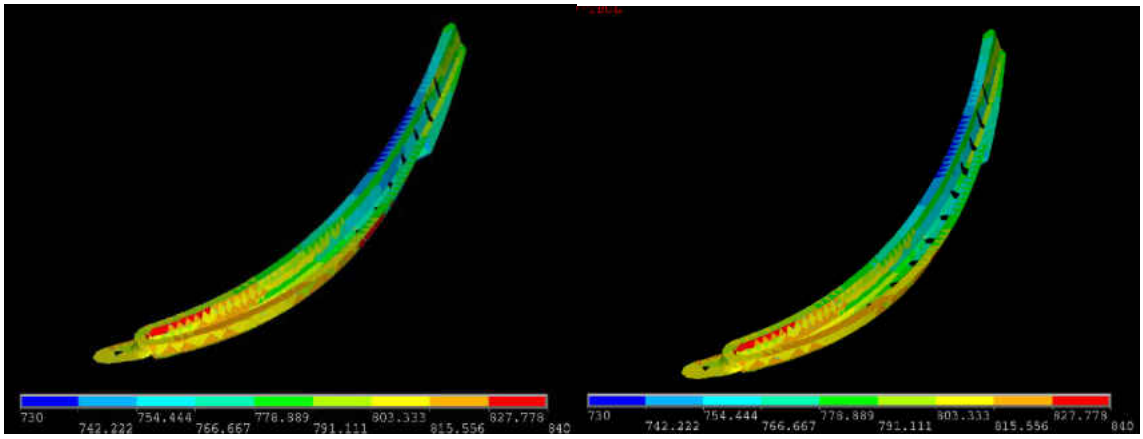

(b)

Figure 25: First and last iteration, (a) tip heat transfer coefficient (mW/mm^2K) (b) tip bulk temperature (^oC)

4.4 Thermo-Elastic Mesh Solution

The material used for the conduction problem is a nickel-base alloy IN738LC. The material properties as a function of temperature are listed in figure 26.

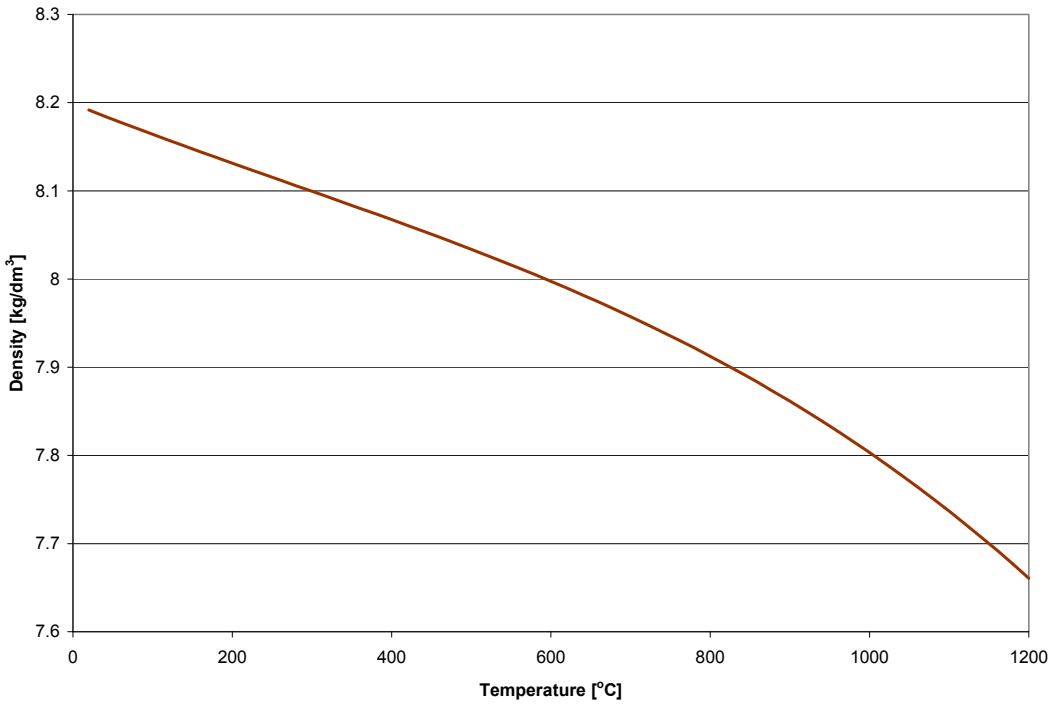

(a)

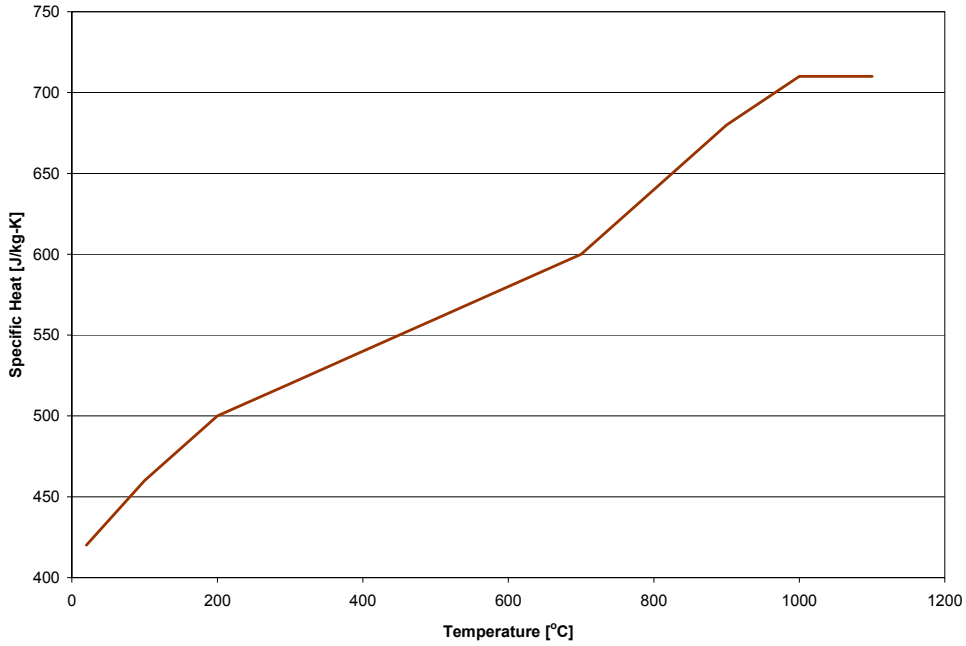

(b)

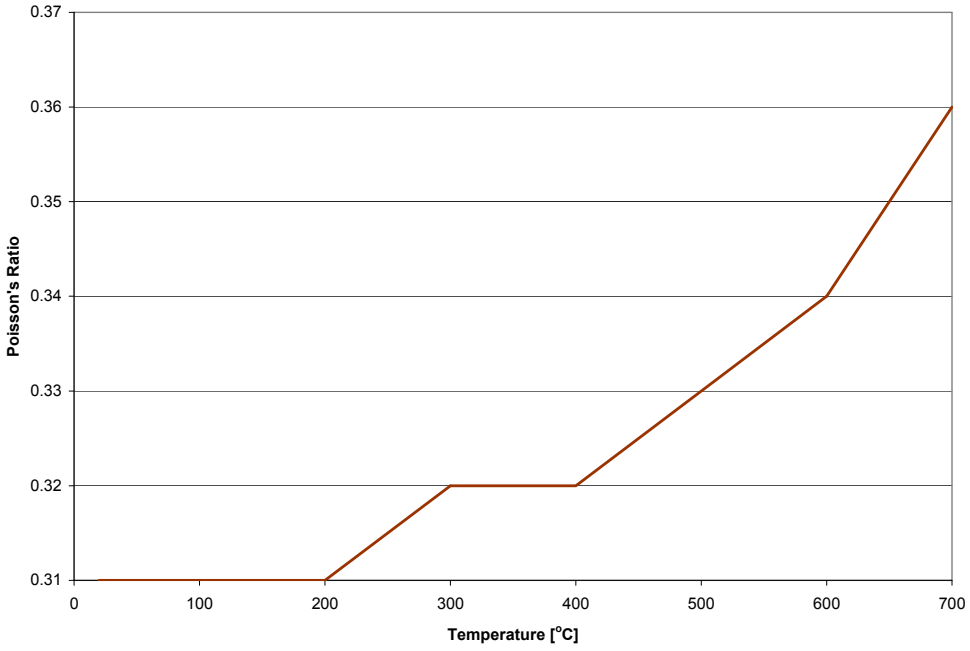

(C)

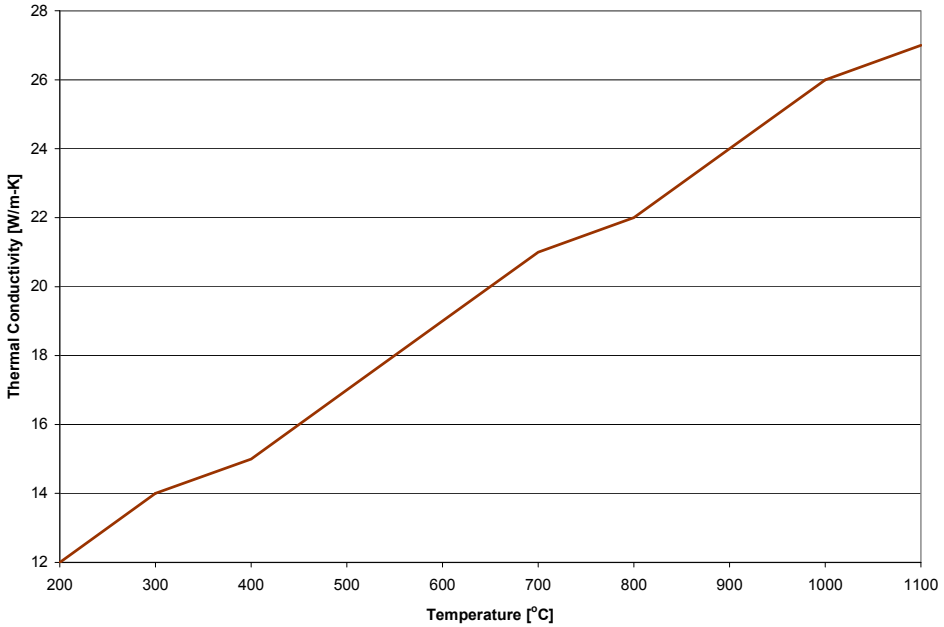

(d)

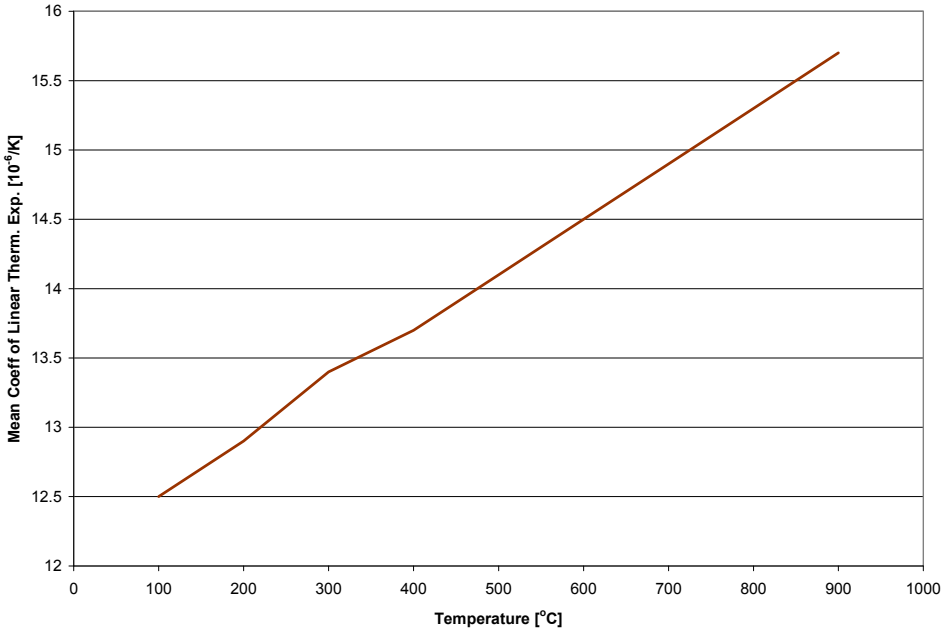

(e)

Figure 26: Material properties IN738LC (a) density (b) specific heat (c) Poisson's ratio (d) thermal conductivity (e) mean coefficient of thermal expansion

The surface metal temperatures distributions along the channels are shown in figure 27. The channel close to the trailing of the airfoil experiences the hottest temperature of 828.853 ^{o}C while the channels at the root of the blade are maintain considerably cooled at 394.682 ^{o}C. The maximum temperature on the last iteration is approximately 113 ^{o}C higher than the first iteration.

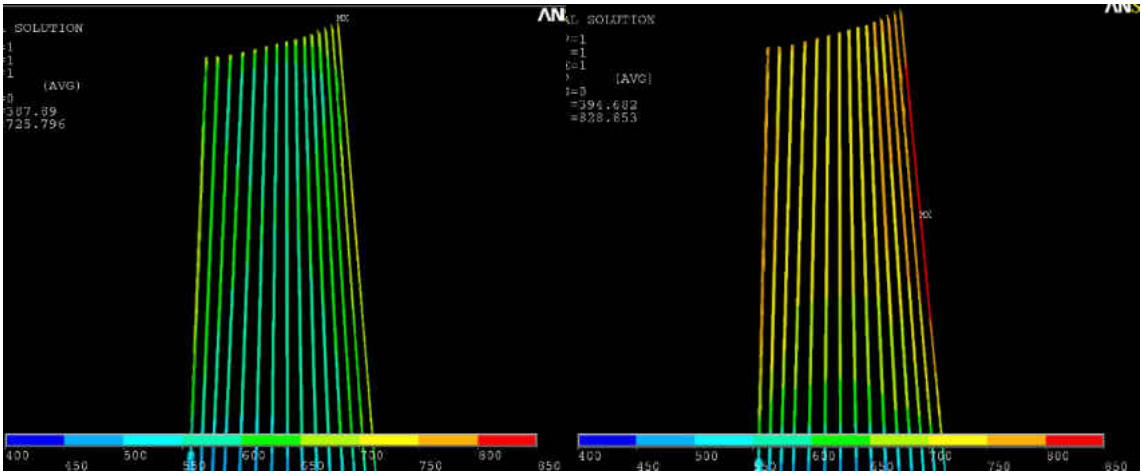

Figure 27: First and last iteration, channels metal temperatures (^{o}C)

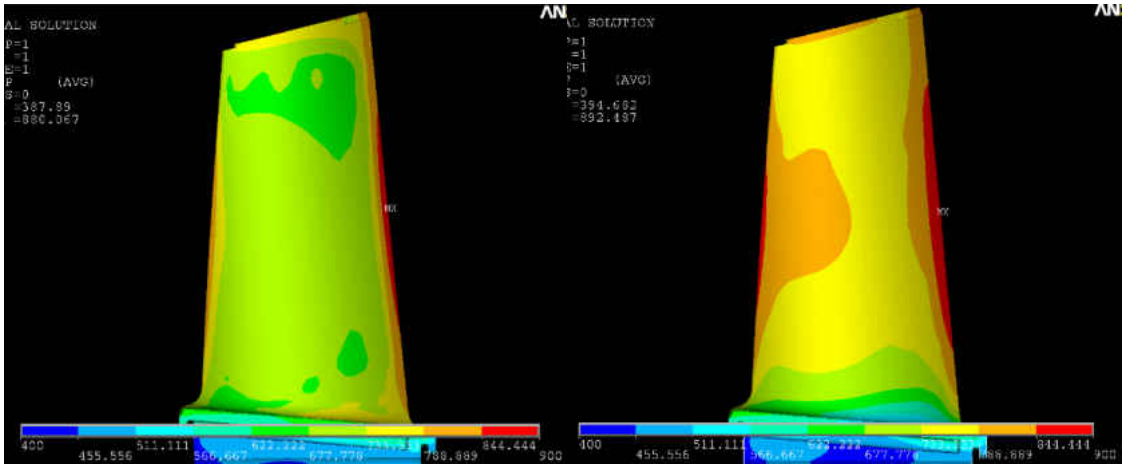

(a)

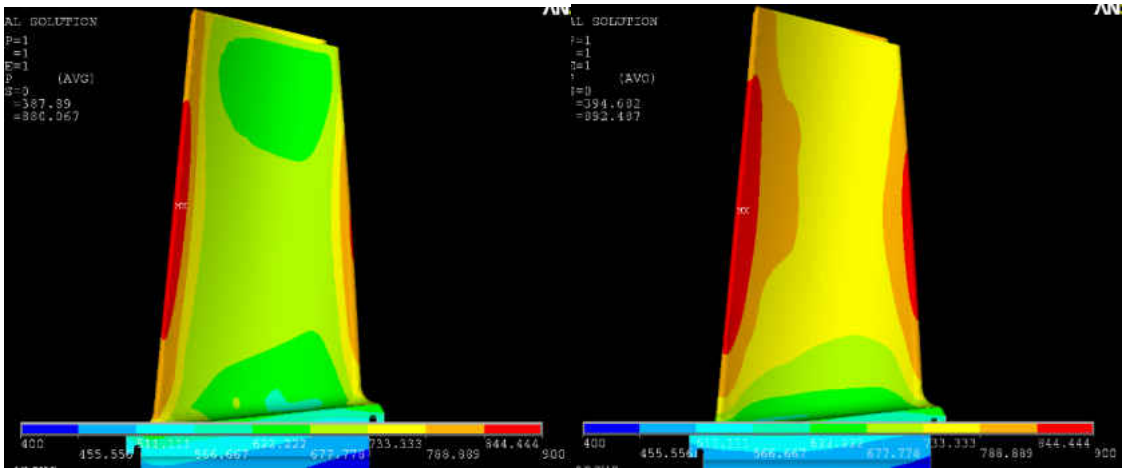

(b)

Figure 28: First and last iteration metal temperatures (^{o}C) (a) airfoil suction side (b) airfoil pressure side

As shown in figure 28 the hottest areas on the blade are the leading edge and trailing edge being the trailing edge the area of maximum temperature with 892.49 ^{o}C. Figure 28 also shows how the contours of higher temperature are more intense on the last iteration than the first one.

The Von Misses stresses are shown in figure 29 and figure 30 shows the blade growth in the x, y, and z directions for the first and last iteration. The maximum displacement obtained in the last iteration in the radial direction is 3.36 mm, 0.211 mm greater than the one obtained in the first iteration.

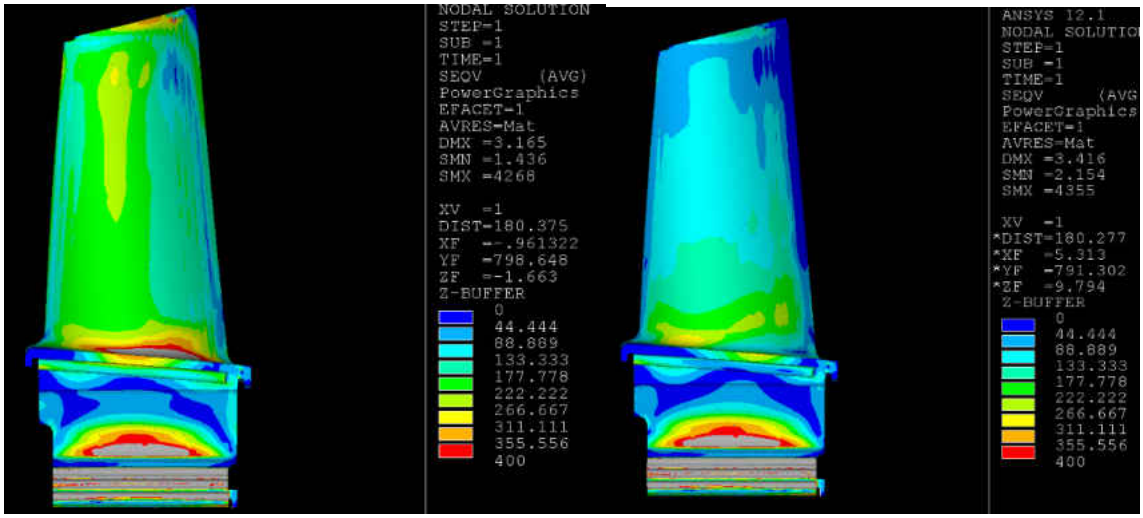

(a)

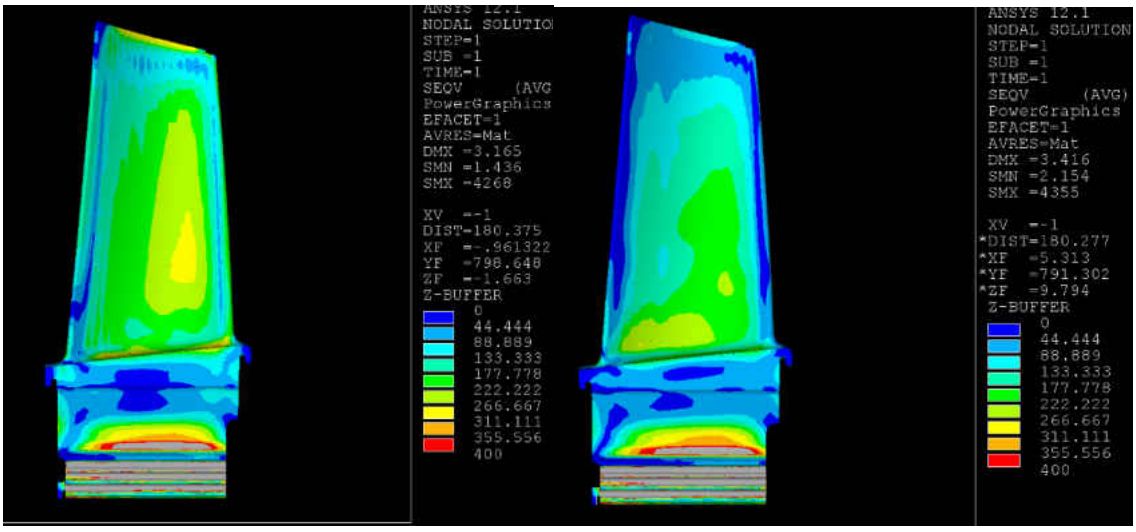

(b)

Figure 29: Von Misses stresses (MPa) (a) airfoil suction side (b) airfoil pressure side

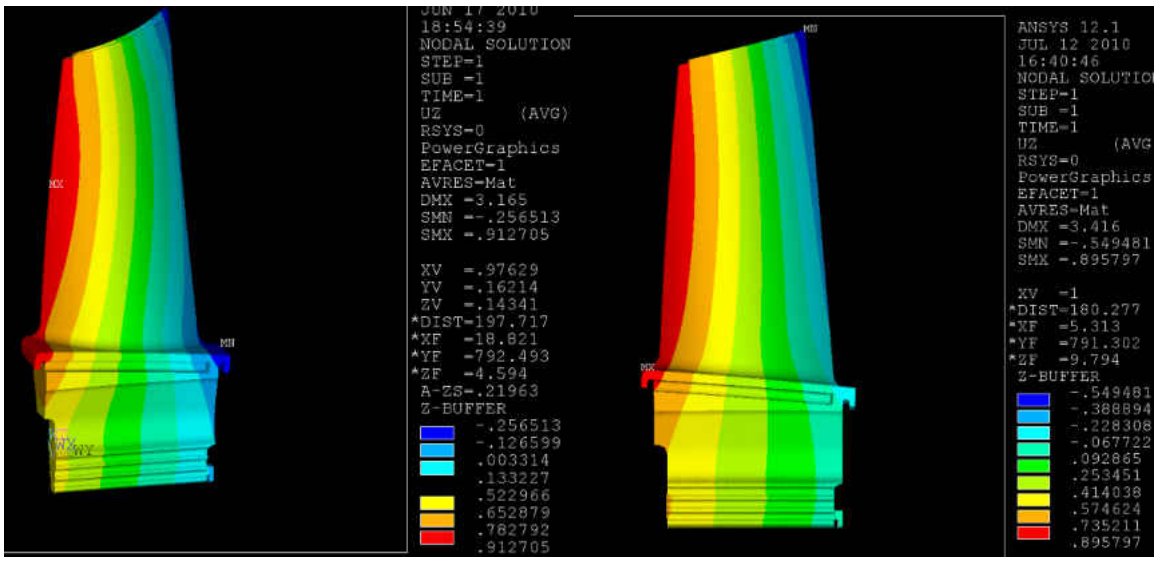

(a)

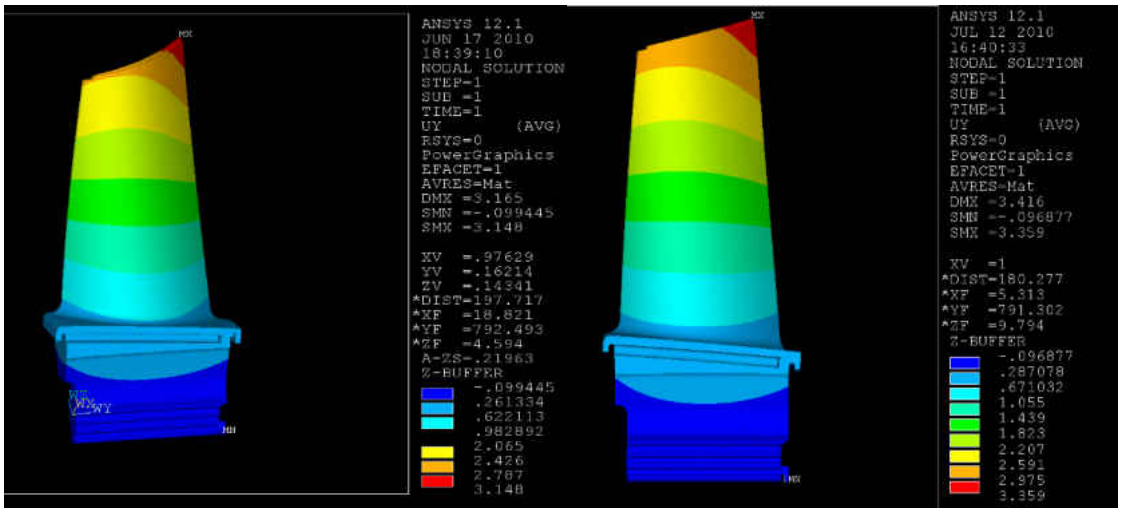

(b)

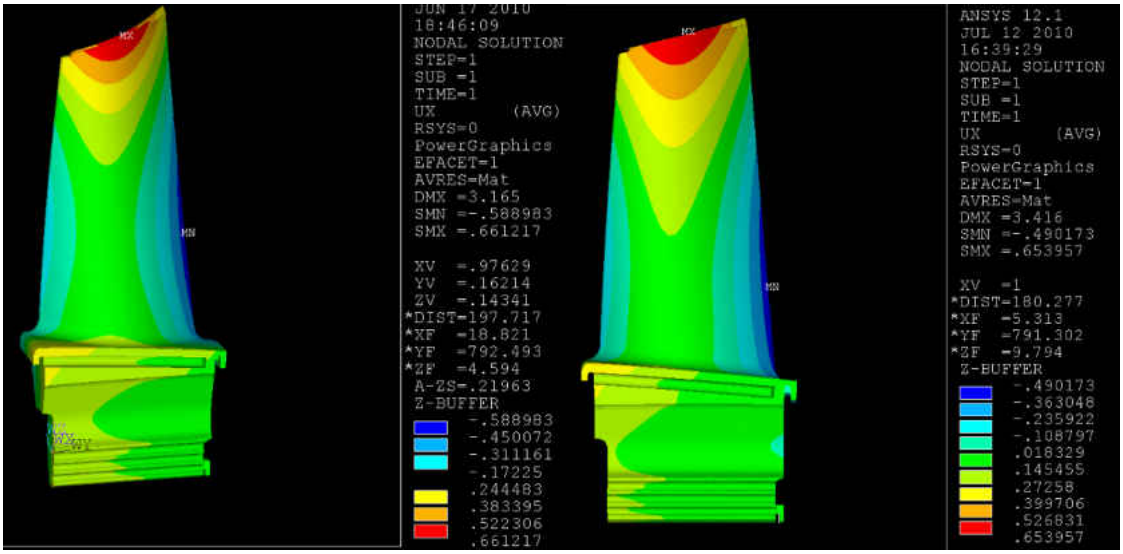

(c)

Figure 30: Blade displacements (mm) (a) z direction (b) y direction (c) x direction

For comparison purposes some nodes from the tip of the blade were selected and their displacements in the radial directions and temperatures are shown in figure 31 and figure 32 respectively. Node number 1 is at the leading edge tip of the blade and node number 14 is at the trailing edge tip of the blade.

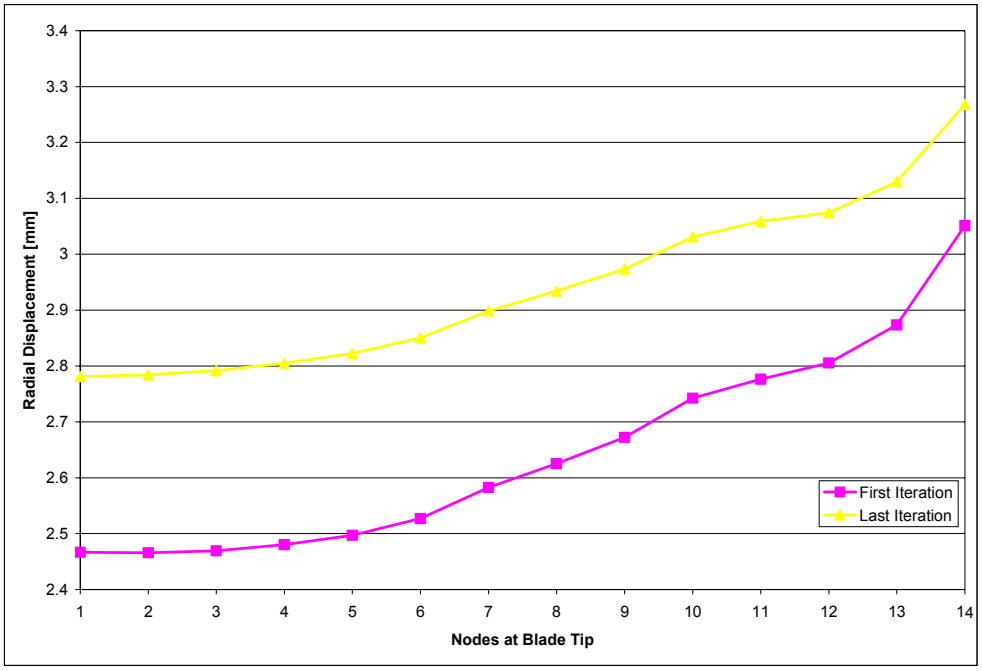

Figure 31: Nodal displacement at blade tip

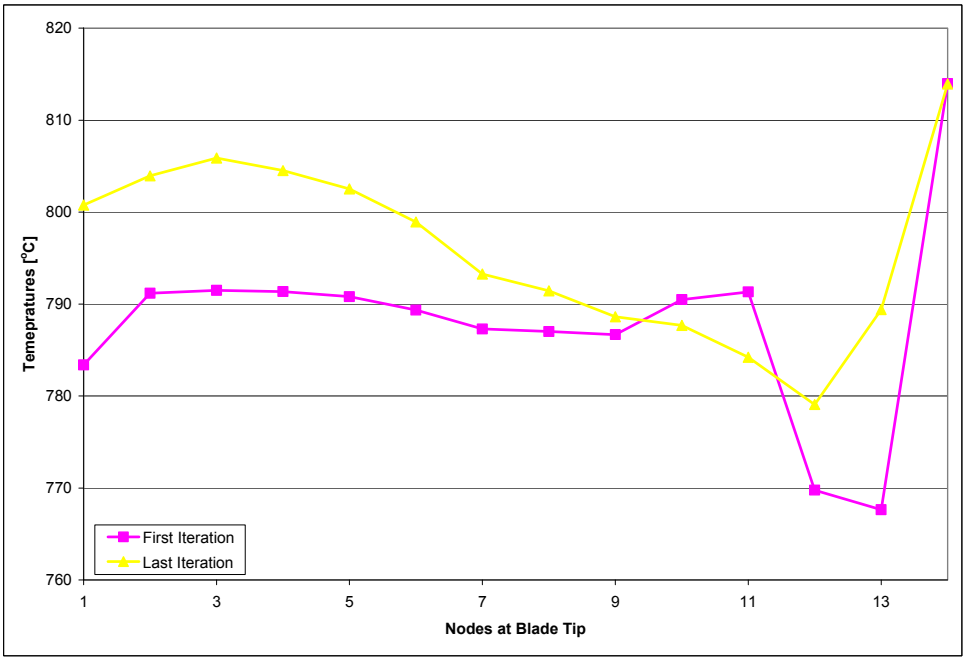

Figure 32: Nodal temperature at blade tip

CHAPTER FIVE: CONCLUSION

Clearances between gas turbine casings and rotating blades is of quite importance on turbo machines since a significant loss of efficiency can occur if the clearances are not predicted accordingly. The radial thermal growths of the blade may be over or under predicted if poor assumptions are made on calculating the metal temperatures of the surfaces exposed to the fluid. The external surface of the blade is exposed to hot gas temperatures and it is internally cooled with air coming from the compressor. This cold air enters the radial channels at the root of the blade and then exists at the tip. To obtain close to realistic metal temperatures on the blade, the Conjugate Heat Transfer (CHT) approach was utilized in this research. The radial thermal growth of the blade was then compared to the initial guess.

This work focused on the interaction between the external boundary conditions obtained from the commercial Computational Fluid Dynamics software package CFX, the internal boundary conditions along the channels from a 1D flow solver proprietary to Siemens Energy, and the 3D metal temperatures and deformation of the blade predicted using the commercial Solid Mechanics software package ANSYS.

An iterative technique to solve CHT problems was demonstrated and discussed. The results of this work helped to highlight the importance of CHT in predicting metal temperatures and the implications it has in other aspect of the gas turbine design such as the tip clearances.

LIST OF REFERENCES

[1] Abram S. Dorfman, "Conjugate Problems In Convective Heat Transfer," CRC Press, 2010

[2] Je-Chin Han, Sandip Dutta, and Srinath V. Ekkad, "Gas Turbine Heat Transfer And Cooling Technology," Taylor & Francis, 2000

[3] Adriam Bejam, "Heat Transfer", John Wiley & Sons, 1993

[4] A. Kassab, E. Divo, J. Heidmann, E. Steinthorsson, F. Rodriguez, "BEM/FVM conjugate heat transfer analysis of a three-dimensional film cooled turbine blade", International Journal of Numerical Methods for Heat and Fluid Flow, Vol. 13 No 5, 2003 pp. 581-610.

[5] E. Divo, E. Steinthorsson, A. Kassab, R. Bialecki, "An iterative BEM/FEM protocol for steady-state multi-dimensional conjugate heat transfer in compressible flows", Engineering Analysis with Boundary Elements, EABE 1354, 2002 pp. 1-8

[6] Eduardo Divo, Alain J. Kassab, "A meshless method for conjugate heat transfer problems", Engineering Analysis with Boundary Elements, EABE 1663, 2004 pp. 1-14

[7] Mahmood Silieti, Eduardo Divo, Alain J. Kassab, "The Effect of Conjugate Heat Transfer on Film Cooling Effectiveness", Numerical heat Transfer, Part B, 56: 335-350, 2009

[8] B. Gamez, D. Ojeda, E. Divo, A. Kassab, M. Cerrolaza, " Parallelized iterative domain decomposition Boundary element method for thermoelasticity in

piecewise non-homogeneous media", Engineering Analysis with Boundary Elements 32 (2008) 1061-1073

[9] Eduardo Divo, Alain Kassab, "Iterative domain decomposition meshless method modeling of incompressible viscous flows and conjugate heat transfer", Engineering Analysis with Boundary Elements 30 (2006) 465-478

[10] Budugur Lakshminarayana, "Fluid Dynamics and Heat Transfer of Turbomachinery", John Wiley & Sons, New York, 1996

[11] William M. Kays, "Michael E. Crawford, "Fluid Dynamics and Heat Transfer of Turbomachinery", McGraw-Hill Book Company, New York, 1980

[12] He M, Kassab AJ, Bishop PJ, Minardi A., " Acoupled FDM/BEM iterative solution for the conjugate heat transfer problem In reply to: thick-walled channels: constant temperature imposed at the outer channel wall", Engng Anal 1995; 15(1):43-50

[13] He M, Bishop P, Kassab AJ, Minardi A. A coupled FDM/BEM solution for the conjugate heat transfer problem" Numer Heat Transfer, Part B: Fundam 1995;11(2):173-81

[14] Kontinos D., "Coupled Thermal analysis method with application to metallic thermal protection panels", AIAA J Thermophys Heat Transfer 1997; 11(2):173-81

[15] ANSYS, Inc., "ANSYS Users Manual", Version 12.1, ANSYS, Canonsburg, Pa, 2009

[16] ANSYS, Inc., "ANSYS CFX Users Manual", Version 12, ANSYS, Canonsburg, Pa, 2009

[17] Heidmann, J.D., Kassab, A.J., Divo, E. Rodriguez, F., and Steinthorsson, E., 2003, "Conjugate Heat Transfer on a Realistic Film Cooled Turbine Vane," ASME paper GT2003-38369

[18] Kassab, A.J., Divo, E., Heidmann, J.D., Steinthorsson, E., and Rodriguez, F., 2003, "BEM/FVM Conjugate Heat Transfer Analysis of a Three-Dimentional Film Cooled Turbine Blade", International Journal for Numerical Methods in Heat Transfer and Fluid Flow, Vol. 13(5), pp.581-610.

[19] Kane J., "Boundary element analysis in engineering continuum mechanics", New Jersey: Prentice-Hall; 1994

[20] Bohn, D.E., Becker, V.J. and Rungen, A.U. (1997), [a]Experimental and numerical conjugate flow and heat transfer investigation of a shower-head cooled turbine guide vane", ASME paper 97-GT-15

[21] Menter, F.R. (1993), "Zonal two-equation κ-ω turbulence models for aerodynamic flows", AIAA paper 93-2906

[22] R. Menter, "Two-equation eddy-viscosity turbulence models for engineering Applications", AIAA J. 32 (8) (1994) 1598–1605

[23] Shyy W, Burke J. Study of iterative characteristics of convective diffusive and conjugate heat transfer problems. Numer Heat Transfer, Part B 1994;26:21-37